The Astrophysical Journal Supplement Series, 168:231–267, 2007 February

THE INTERSTELLAR MEDIUM OF GAMMA-RAY BURST HOST GALAXIES. I. ECHELLE SPECTRA OF *SWIFT* GRB AFTERGLOWS

J. X. Prochaska,[1] H.-W. Chen,[2] J. S. Bloom,[3] M. Dessauges-Zavadsky,[4] J. M. O'Meara,[5] R. J. Foley,[3] R. Bernstein,[6] S. Burles,[7] A. K. Dupree,[8,9] E. Falco,[8] and I. B. Thompson[9,10]

Received 2006 May 23; accepted 2006 October 9

ABSTRACT

We present optical echelle spectra of four gamma-ray burst (GRB) afterglows (GRB 050730, GRB 050820, GRB 051111, and GRB 060418) discovered during the first 1.5 yr of operation of the *Swift* satellite and localized by either the *Swift* telescope or follow-up ground-based imaging. We analyze the spectra to derive accurate column density measurements for the transitions arising in the interstellar medium (ISM) of the GRB host galaxies. These measurements can be used to constrain the physical properties of the ISM, including the metallicity, dust-to-gas ratio, ionization state, and chemical abundances of the gas. We also present measurements of the strong Mg II systems in the GRB afterglow spectra. With the publication of this paper, we provide the first data release of echelle afterglow spectra by the GRAASP collaboration to the general community.

Subject headings: galaxies: ISM — gamma rays: bursts

Online material: color figures

1. INTRODUCTION

The launch of the *Swift* satellite (Gehrels et al. 2004) has revolutionized the study of the interstellar medium of gamma-ray burst (GRB) host galaxies and fostered new studies on the intervening intergalactic medium (Chen et al. 2005; Prochter et al. 2006). While previous missions alerted the community to the existence of very bright GRB afterglows (e.g., Kulkarni et al. 1999), only a few events were identified in time to allow echelle observations (Fiore et al. 2005). The rapid localization by *Swift* of the hard X-ray emission to several arcminutes (Barthelmy et al. 2005) and the soft X-ray component to a few arcseconds (Osborne et al. 2005) has enabled observers to obtain high signal-to-noise, high-resolution spectroscopy of GRBs with 10 m class telescopes.

In this paper, we present a uniform data set of echelle spectra of four GRB afterglows by our GRB Afterglows as Probes (GRAASP[11]) collaboration. Among other applications, the data presented here can be used to derive constraints on the physical conditions of the interstellar medium (ISM) of GRB host galaxies: the metallicity, dust-to-gas ratio, chemical abundance patterns, ionization state, the distance of the GRB to the absorbing gas, etc. Future papers in this series will examine these properties in greater detail and provide comparison with analogous observations along quasar sight lines. In addition to the data presented here, we have collected several low-resolution spectra of these and other GRBs and will present that data in a companion paper (J. Prochaska et al. 2007, in preparation) along with ISM abundance measurements obtained by different analysis techniques more suitable to lower resolution data (Prochaska 2006).

We also present measurements of the strong Mg II systems in the GRB afterglow spectra. In § 2 we summarize the observations and data reduction procedures. The methodology is briefly described in § 3 and the line profiles and column density values are given in §§ 4 and 5.

2. OBSERVATIONS AND DATA REDUCTION

The GRB afterglow spectra presented here were acquired with either the High Resolution Echelle Spectrometer (HIRES; Vogt et al. 1994) on the Keck I 10 m telescope or the Magellan Inamori Kycoera Echelle spectrometer (MIKE; Bernstein et al. 2003) on the Magellan 6.5 m Clay telescope at Las Campanas Observatory. Table 1 presents a summary of the GRB events, the afterglow observations, instrumental configurations, and data quality of the spectra obtained for the four afterglows for which we have obtained high-resolution spectra: GRB 050730, GRB 050820, GRB 051111, and GRB 060418.

The data were reduced with the HIRES Redux[12] and MIKE Redux[13] pipelines (S. Burles, J. Prochaska, & R. Bernstein 2007, in preparation). Briefly, the two-dimensional (2D) images were bias-subtracted, flat-fielded, and wavelength-calibrated using standard ThAr and quartz lamp calibration images. The data were optimally extracted using a nonparametric spatial profile and coadded after weighting by the global SNR^2 of each echelle order. A final, normalized one-dimensional (1D) spectrum was produced by fitting high-order Legendre polynomials to each echelle order (HIRES) or the fluxed 1D spectrum (MIKE).

We provide additional details related to the specific observations in the following section.

3. METHODS: COLUMN DENSITY MEASUREMENTS

Following our standard practice for the analysis of interstellar lines observed in the damped Lyα systems (quasar absorption

[1] UCO/Lick Observatory, University of California, Santa Cruz, CA; xavier@ucolick.org.
[2] Department of Astronomy, University of Chicago, Chicago, IL; hchen@oddjob.uchicago.edu.
[3] Department of Astronomy, University of California, Berkeley, CA.
[4] Observatoire de Genève, Sauverny, Switzerland.
[5] Department of Physics, Penn State Worthington Scranton, Dunmore, PA.
[6] Department of Astronomy, University of Michigan, Ann Arbor, MI.
[7] MIT Kavli Institute for Astrophysics and Space Research, Massachusetts Institute of Technology, Cambridge, MA.
[8] Harvard-Smithsonian Center for Astrophysics, Cambridge, MA.
[9] This paper includes data gathered with the 6.5 m Magellan Telescopes located at Las Campanas Observatory.
[10] Observatories of the Carnegie Institution of Washington, Pasadena, CA.
[11] See http://www.graasp.org.
[12] See http://www2.keck.hawaii.edu/inst/hires/.
[13] See http://web.mit.edu/~burles/www/MIKE/.

TABLE 1
Observation Log

GRB	UT_{burst}	z_{GRB}	Telescope	Instr.	FWHM (km s^{-1})	UT_{start}	UT_{end}	AM[a]	λ (Å)	SNR[b]
050730.....	19:58:23	3.969	Magellan/Clay	MIKE	12	2005 Jul 31 00:00:04	2005 Jul 31 00:30:04	1.23	3400–9400	11
					12	2005 Jul 31 00:32:52	2005 Jul 31 01:02:52	1.33	3400–9400	10
					12	2005 Jul 31 01:05:11	2005 Jul 31 01:35:11	1.48	3400–9400	8
050820.....	06:34:53	2.615	Keck I	HIRESr	7.5	2005 Aug 20 07:28:59	2005 Aug 20 07:43:59	1.51	3800–8000	14
					7.5	2005 Aug 20 07:44:42	2005 Aug 20 07:59:43	1.41	3800–8000	12
051111.....	05:59:39	1.549	Keck I	HIRESr	5	2005 Aug 11 07:02:58	2005 Aug 11 07:32:59	1.02	4160–8720	22
					5	2005 Aug 11 07:34:23	2005 Aug 11 08:04:23	1.06	4160–8720	18
					5	2005 Aug 11 08:05:22	2005 Aug 11 08:35:23	1.12	4160–8720	14
060418.....	03:06:08	4.048	Magellan/Clay	MIKE	12	2006 Apr 18 03:34:02	2006 Apr 18 03:54:02	1.61	3400–9400	21
					12	2006 Apr 18 04:01:08	2006 Apr 18 04:31:08	1.44	3400–9400	17
					12	2006 Apr 18 04:54:31	2006 Apr 18 05:24:31	1.24	3400–9400	9

[a] Air mass at the start of the observation.
[b] Signal-to-noise ratio per resolution element (FWHM) near the center of the spectral range.

systems with $N_{H\,II} > 2 \times 10^{20}$ cm^{-2} Prochaska et al. 2001, 2003), we have measured column densities using the apparent optical depth method (AODM; Savage & Sembach 1991). This technique leads to nonparametric, accurate results provided the profiles are resolved. In cases where one measures multiple transitions for a single ion (e.g., Ni II 1741, 1751), one can test for line saturation by examining the column density values derived as a function of the line strength. If there is no trend of increasing column density with decreasing line strength, then the profiles are free of significant "hidden" saturation (Jenkins 1996).

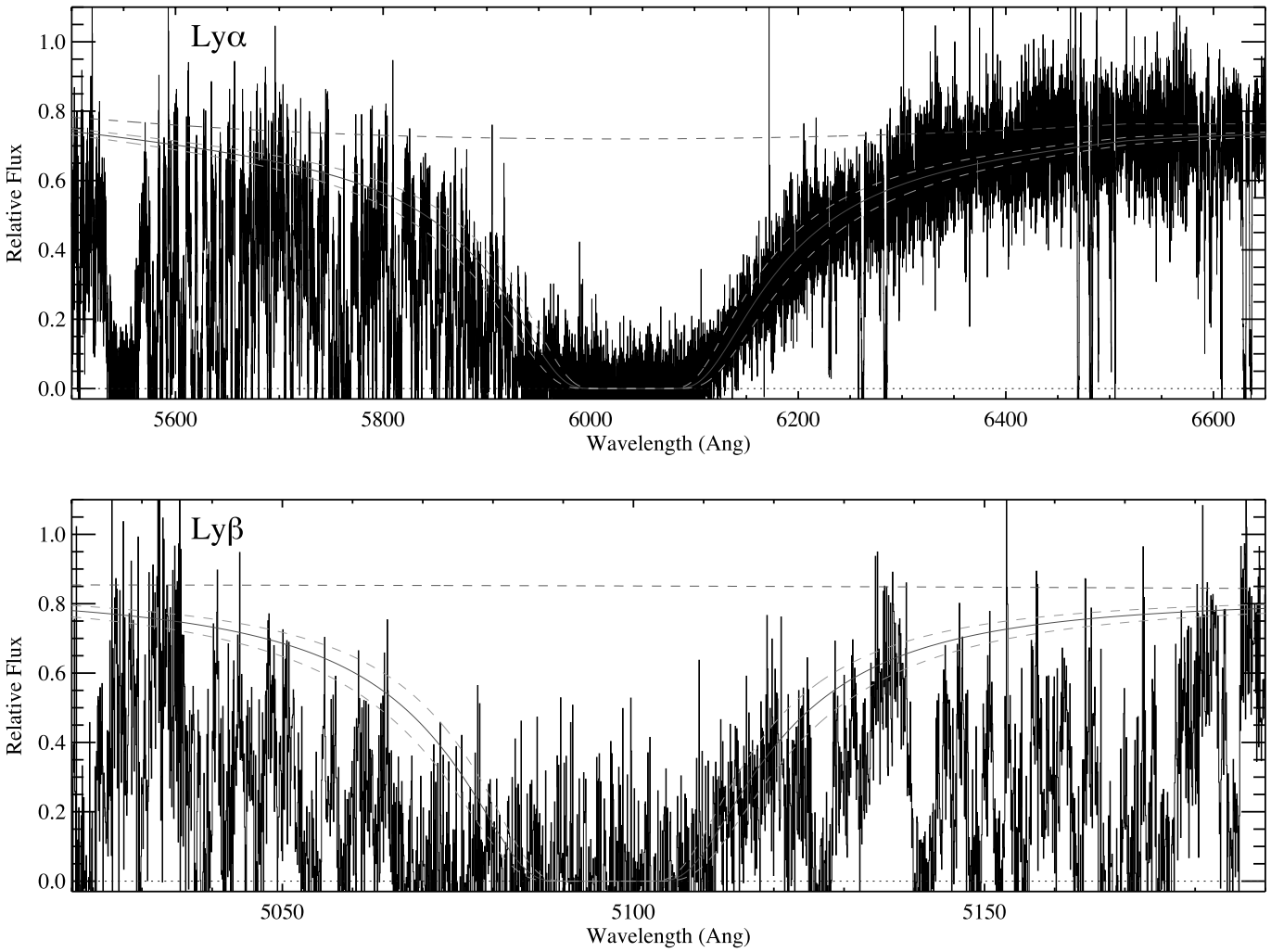

Fig. 1.—Lyα and Lyβ transitions for the host galaxy of GRB 050730. The dashed purple line above the data shows our best guess at the afterglow continuum. The curves overplotted on the data show the Voigt profiles for our favored solution ($\log N_{H\,II} = 22.15 \pm 0.10$ dex). [*See the electronic edition of the Supplement for a color version of this figure.*]

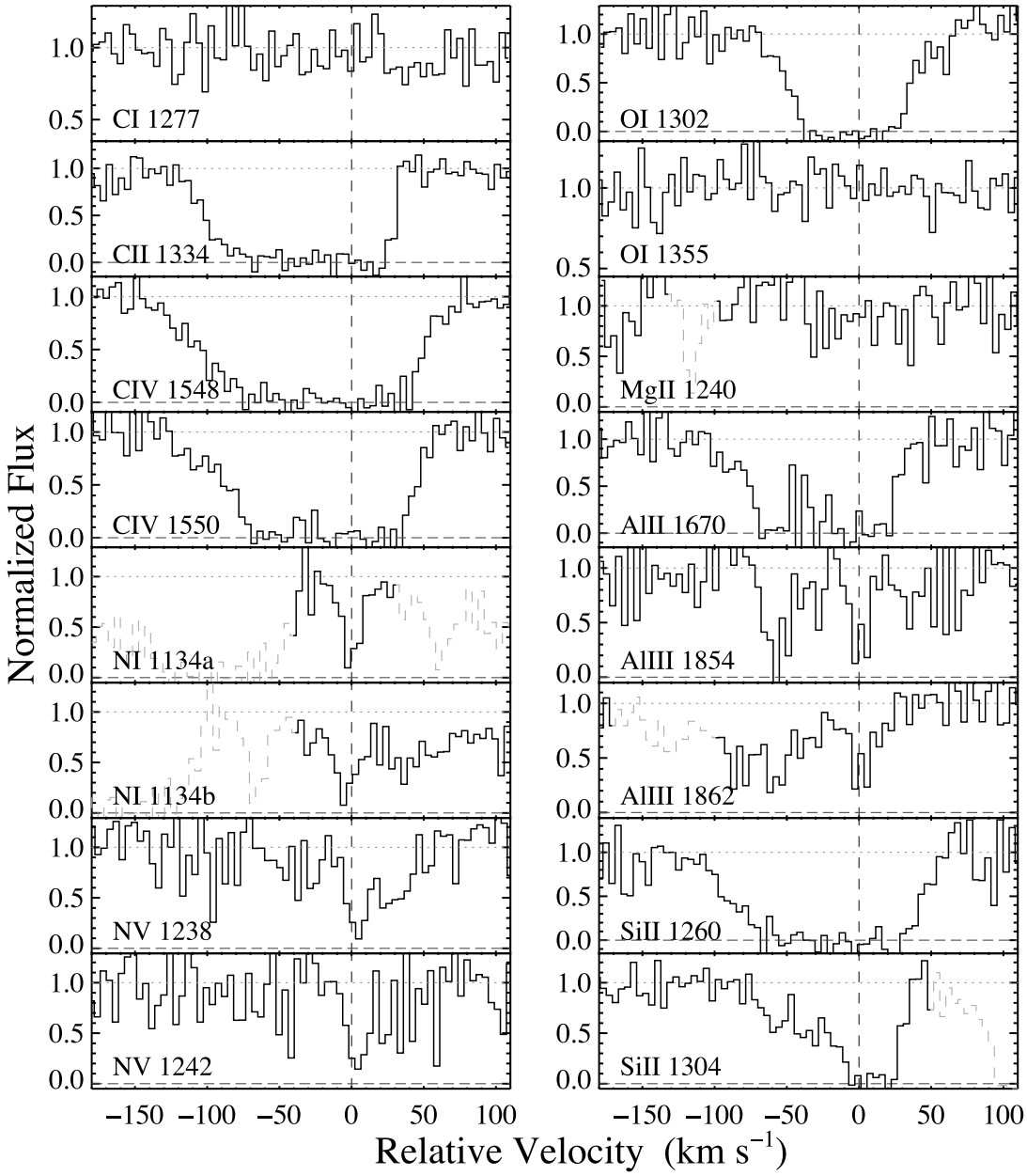

FIG. 2.—Velocity profiles of the resonance transitions identified in the ISM of the host galaxy of GRB 050730. The velocity $v = 0$ km s^{-1} corresponds to $z = 3.96855$. The profiles are ordered by atomic number and ionization state. [*See the electronic edition of the Supplement for a color version of this figure.*]

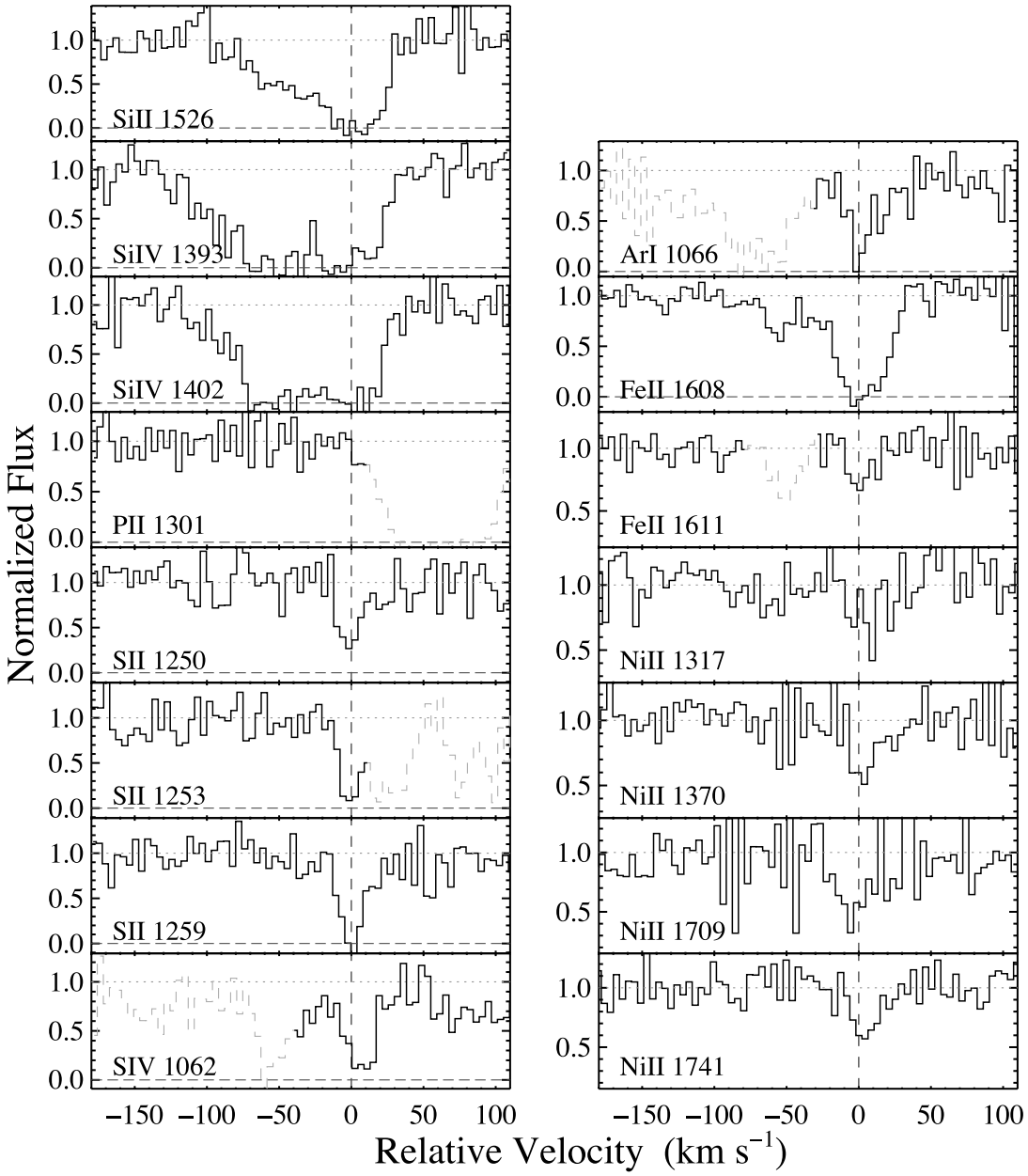

FIG. 2—*Continued*

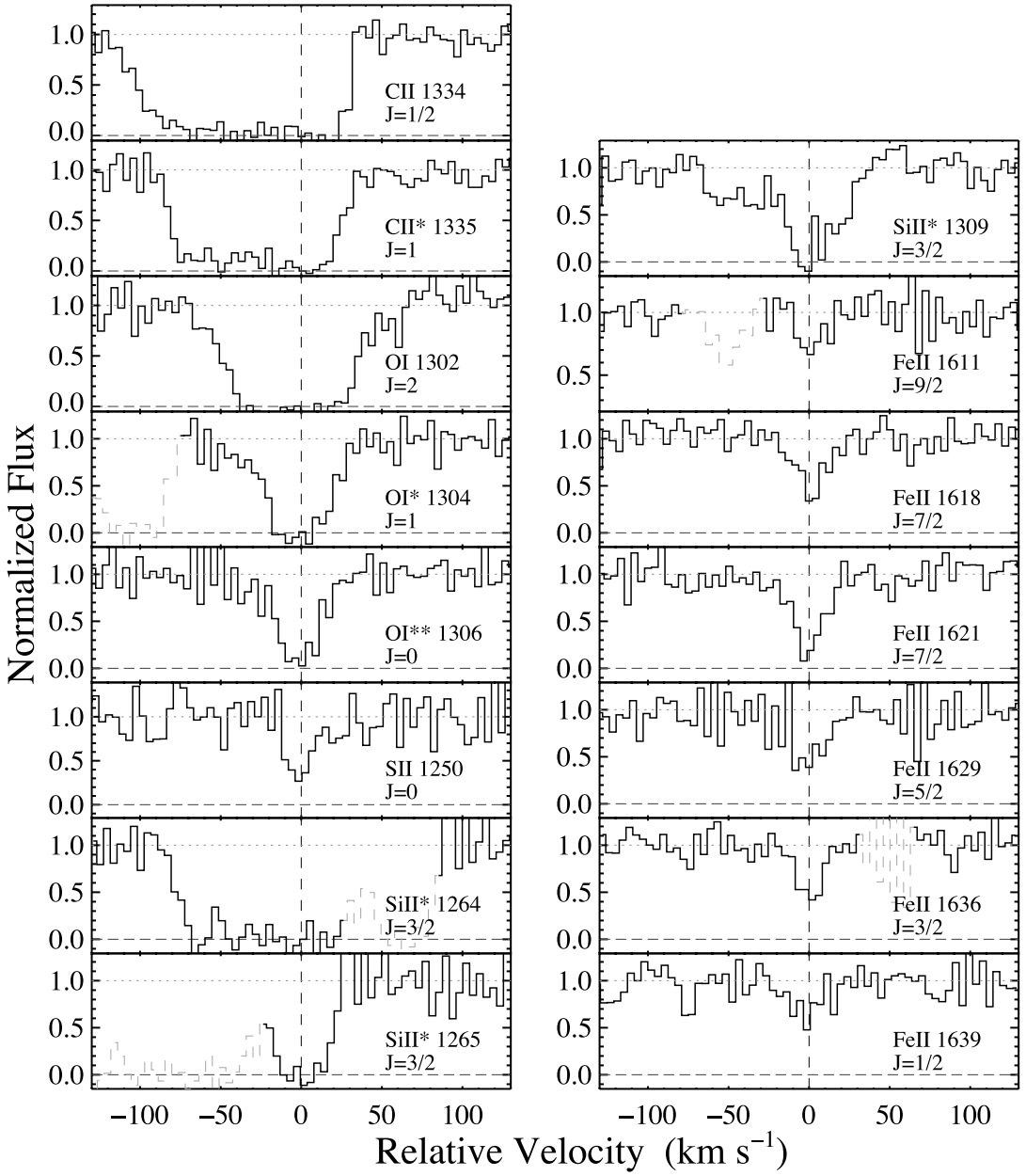

FIG. 3.—Velocity profiles of the fine-structure transitions (with several resonance lines for comparison) identified in the ISM of the host galaxy of GRB 050730. The velocity $v = 0$ km s^{-1} corresponds to $z = 3.96855$. The profiles are ordered by atomic number and energy level. [*See the electronic edition of the Supplement for a color version of this figure.*]

We find no indication of hidden saturation in the GRB studied here.

We report column density values for all transitions detected at greater than 3 σ statistical significance and report 1 σ statistical uncertainty in the sections that follow. For ions or atoms where multiple transitions are measured, we report the weighted mean column density and combined statistical error in that mean. While the data may formally yield errors of less than 0.01 dex, we recommend that one adopt a minimum statistical uncertainty of 5% the column density. Saturated line profiles, i.e., those where the minimum normalized flux of the line profile is less than the 1 σ statistical error, are reported as lower limits. Finally, undetected or blended transitions are reported as 3 σ upper limits assuming statistical uncertainty alone. Accounting for continuum error, these limits are more likely 2 σ values. We note that uncertainties in weak lines are likely to be dominated by systematics associated with the continuum placement, and therefore adopt a minimum uncertainty of 5% in our own analysis.

The AODM technique cannot be applied to transitions that are blended with coincident features. In cases of particular importance, we have derived line profile fits to the data using the software package VPFIT, kindly provided by R. Carswell. Finally, when the Lyα profile is covered by the spectroscopic observations, we have fitted this line using the `x_fitdla` algorithm within the XIDL package[14] (e.g., Prochaska et al. 2005).

The following sections present velocity profiles of transitions observed along the GRB sight lines. The transitions are separated into two groups: those arising from the ground state (termed resonance lines) and those arising from excited levels (ambiguously termed fine-structure lines). In all of the figures, line blends are

[14] See http://www.ucolick.org/~xavier/IDL.

TABLE 2
IONIC COLUMN DENSITIES FOR HG 050730

Ion	J[a]	E_J (cm^{-1})	λ (Å)	log f	$v_{\rm int}$[b] (km s^{-1})	W_λ[c] (mÅ)	log N	log $N_{\rm adopt}$
C I	0	0.00	1277.2450	−1.0148	[−40, 40]	<20.0	<13.37	<13.37
	0	0.00	1656.9283	−0.8523	[−30, 50]	<20.4	<13.47	
C II	1/2	0.00	1334.5323	−0.8935	[−150, 50]	577.3 ± 11.4	>14.95	>14.95
	3/2	63.40	1335.7077	−0.9397	[−100, 50]	452.4 ± 9.9	>14.85	>14.85
C IV		0.00	1548.1950	−0.7194	[−150, 70]	807.3 ± 13.7	>14.79	>15.02
		0.00	1550.7700	−1.0213	[−150, 70]	685.1 ± 16.0	>15.02	
N I		0.00	1134.1653	−1.8722	[−30, 30]	67.6 ± 7.3	14.86 ± 0.08	14.78 ± 0.05
		0.00	1134.4149	−1.5714	[−30, 30]	106.4 ± 8.4	14.75 ± 0.07	
N V		0.00	1238.8210	−0.8041	[−40, 80]	142.1 ± 21.3	14.03 ± 0.10	14.09 ± 0.08
		0.00	1242.8040	−1.1066	[−40, 80]	94.1 ± 21.3	14.26 ± 0.11	
O I	2	0.00	1302.1685	−1.3110	[−90, 60]	412.9 ± 10.3	>15.27	>15.27
	2	0.00	1355.5977	−5.9066	[−40, 40]	<16.6	<18.09	
	1	158.26	1304.8576	−1.3118	[−60, 50]	228.8 ± 8.7	>14.94	>14.94
	0	226.98	1306.0286	−1.3122	[−60, 50]	125.0 ± 9.2	>14.61	>14.61
Mg II		0.00	1239.9253	−3.1986	[−40, 40]	<35.4	<16.08	<16.08
		0.00	1240.3947	−3.4498	[−40, 40]	<34.7	<16.15	
Al II		0.00	1670.7874	0.2742	[−110, 50]	590.1 ± 20.7	>13.54	>13.54
Si II	1/2	0.00	1260.4221	0.0030	[−150, 60]	592.1 ± 14.5	>14.08	>14.69
	1/2	0.00	1304.3702	−1.0269	[−90, 50]	291.5 ± 9.8	>14.69	
	1/2	0.00	1526.7066	−0.8962	[−130, 50]	365.5 ± 13.9	>14.55	
	1/2	0.00	1808.0126	−2.6603	[−60, 40]	<30.6	<15.59	
	3/2	287.24	1264.7377	−0.0441	[−100, 40]	469.6 ± 13.3	>14.03	>14.56
	3/2	287.24	1265.0020	−0.9983	[−30, 40]	184.4 ± 11.1	>14.56	
	3/2	287.24	1309.2757	−0.8333	[−75, 50]	205.2 ± 11.1	>14.28	
	3/2	287.24	1817.4512	−3.8894	[−40, 40]	<24.8	<16.03	
Si IV		0.00	1393.7550	−0.2774	[−150, 50]	545.8 ± 16.1	>14.21	>14.52
		0.00	1402.7700	−0.5817	[−150, 50]	505.9 ± 13.6	>14.52	
P II	1/2	0.00	1301.8740	−1.7620	[−40, 20]	<14.6	<14.23	<14.23
S II		0.00	1250.5840	−2.2634	[−30, 55]	58.6 ± 14.7	15.09 ± 0.10	15.22 ± 0.06
		0.00	1253.8110	−1.9634	[−30, 55]	175.4 ± 10.9	15.39 ± 0.07	
		0.00	1259.5190	−1.7894	[−30, 55]	129.2 ± 11.1	>15.07	
Ar I		0.00	1066.6600	−1.1709	[−30, 30]	90.2 ± 8.2	>14.38	>14.38
Fe II	9/2	0.00	1608.4511	−1.2366	[−100, 50]	287.0 ± 10.7	>14.72	14.98 ± 0.12
	9/2	0.00	1611.2005	−2.8665	[−30, 30]	24.2 ± 7.6	14.98 ± 0.12	
	7/2	384.79	1618.4680	−1.6696	[−30, 30]	65.4 ± 8.3	14.26 ± 0.06	14.29 ± 0.04
	7/2	384.79	1621.6856	−1.4191	[−30, 30]	111.2 ± 9.0	14.34 ± 0.07	
	5/2	667.68	1629.1596	−1.4353	[−30, 30]	78.6 ± 11.6	14.12 ± 0.07	14.12 ± 0.07
	3/2	862.61	1634.3498	−1.6882	[−30, 30]	30.3 ± 9.4	13.95 ± 0.11	13.92 ± 0.06
	3/2	862.61	1636.3313	−1.3925	[−30, 30]	57.7 ± 9.0	13.91 ± 0.07	
	1/2	977.05	1639.4012	−1.2373	[−30, 30]	48.5 ± 8.3	13.65 ± 0.07	13.65 ± 0.07
Ni II		0.00	1317.2170	−1.2366	[−40, 40]	<21.0	13.68 ± 0.13	13.68 ± 0.06
		0.00	1370.1310	−1.1141	[−40, 50]	46.8 ± 10.7	13.68 ± 0.09	
		0.00	1741.5490	−1.3696	[−40, 40]	43.2 ± 12.3	13.69 ± 0.11	

[a] Total angular momentum of the electron spin and orbital angular moment. The quantity E_J is the energy above the ground state.
[b] Velocity interval over which the equivalent width and column density are measured.
[c] Rest equivalent width.

indicated by dotted lines. In cases where the line blending is extremely severe, we have not shown the velocity profile.

The atomic data used here have been taken from recent laboratory measurements and theoretical calculations when lab measurements are not available (see Morton 1991, 2003; Bergeson & Lawler 1993; Bergeson et al. 1994, 1996; Tripp et al. 1996; Raassen & Uylings 1998).

4. THE ISM OF GRB HOST GALAXIES

4.1. *GRB 050730*

The *Swift* BAT instrument triggered on GRB 050730 at UT 2005 July 30 19:58:23 and shortly after Holland et al. (2005) reported the detection of a bright optical afterglow ($V = 17.6$ at 199s after the trigger) at R.A. $= 14^{\rm h}08^{\rm m}16.2^{\rm s}$, decl. $= -03^\circ45'41''$. After waiting for the Sun to set at Las Campanas Observatory, we began acquiring data with the Magellan telescope under good conditions. Chen et al. (2005) presented a preliminary analysis of this data set; we present the full set of transitions observed.

Figure 1 presents the Lyα and Lyβ profiles for the host galaxy, and the best Voigt profile fit, which gives $\log N_{\rm H\,II} = 21.15 \pm 0.10$ dex. The uncertainty in this fit is dominated by the fluxing error associated with echelle spectrometers and continuum fitting. A lower resolution, well-calibrated, single-order spectrum would likely give a more precise result.

Figure 2 shows the velocity profiles for the resonance lines associated with the ISM of the host galaxy for GRB 050730. Figure 3 shows the fine-structure transitions and a resonance line for comparison. Finally, Table 2 lists the column density measurements for all of the transitions.

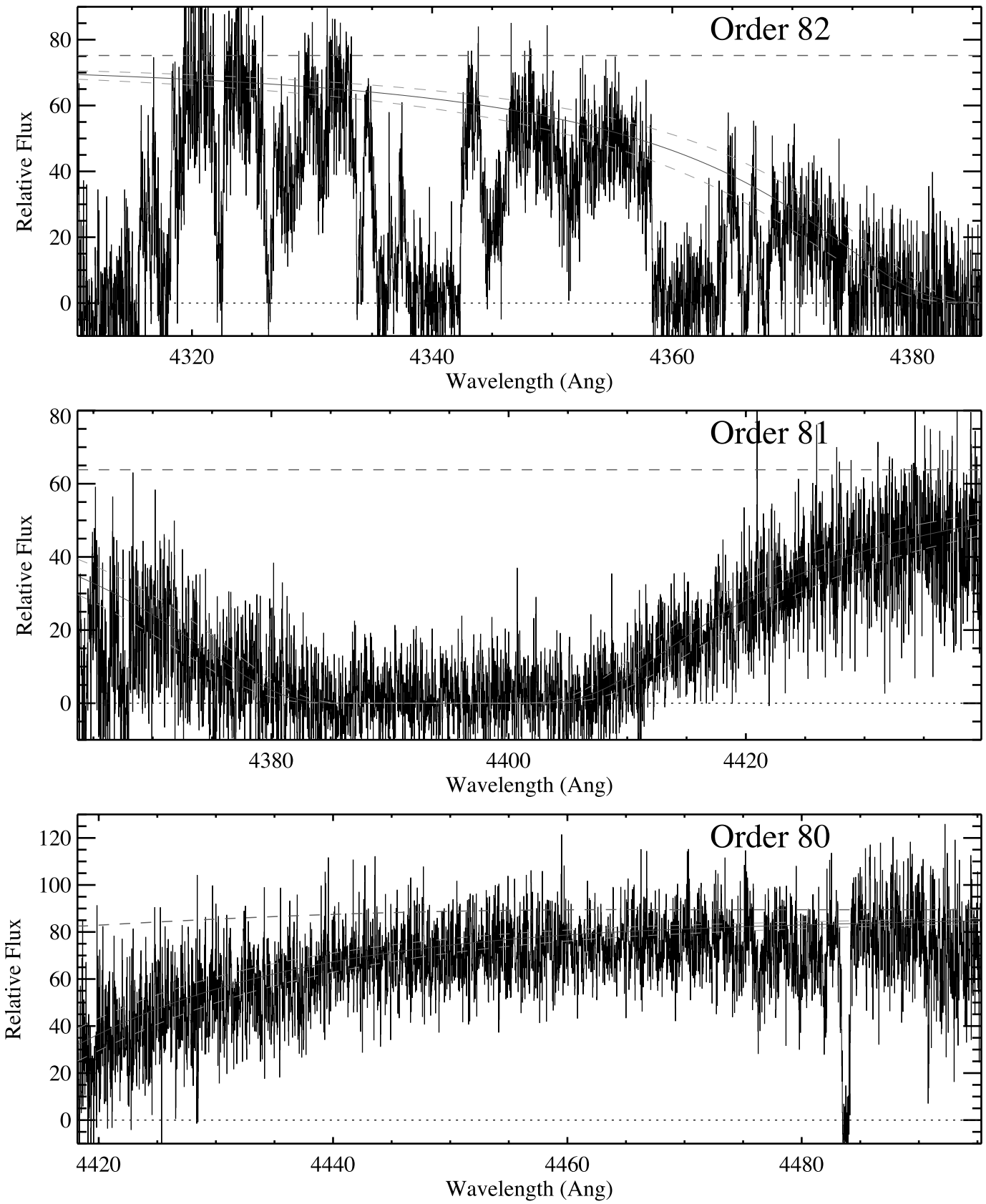

FIG. 4.—Echelle orders covering the Lyα transition for the host galaxy of GRB 050820. The dashed purple line above the data shows our best guess at the afterglow continuum. The curves overplotted on the data show the Voigt profiles for our favored solution ($\log N_{\rm H\,II} = 21.00 \pm 0.10$ dex). [*See the electronic edition of the Supplement for a color version of this figure.*]

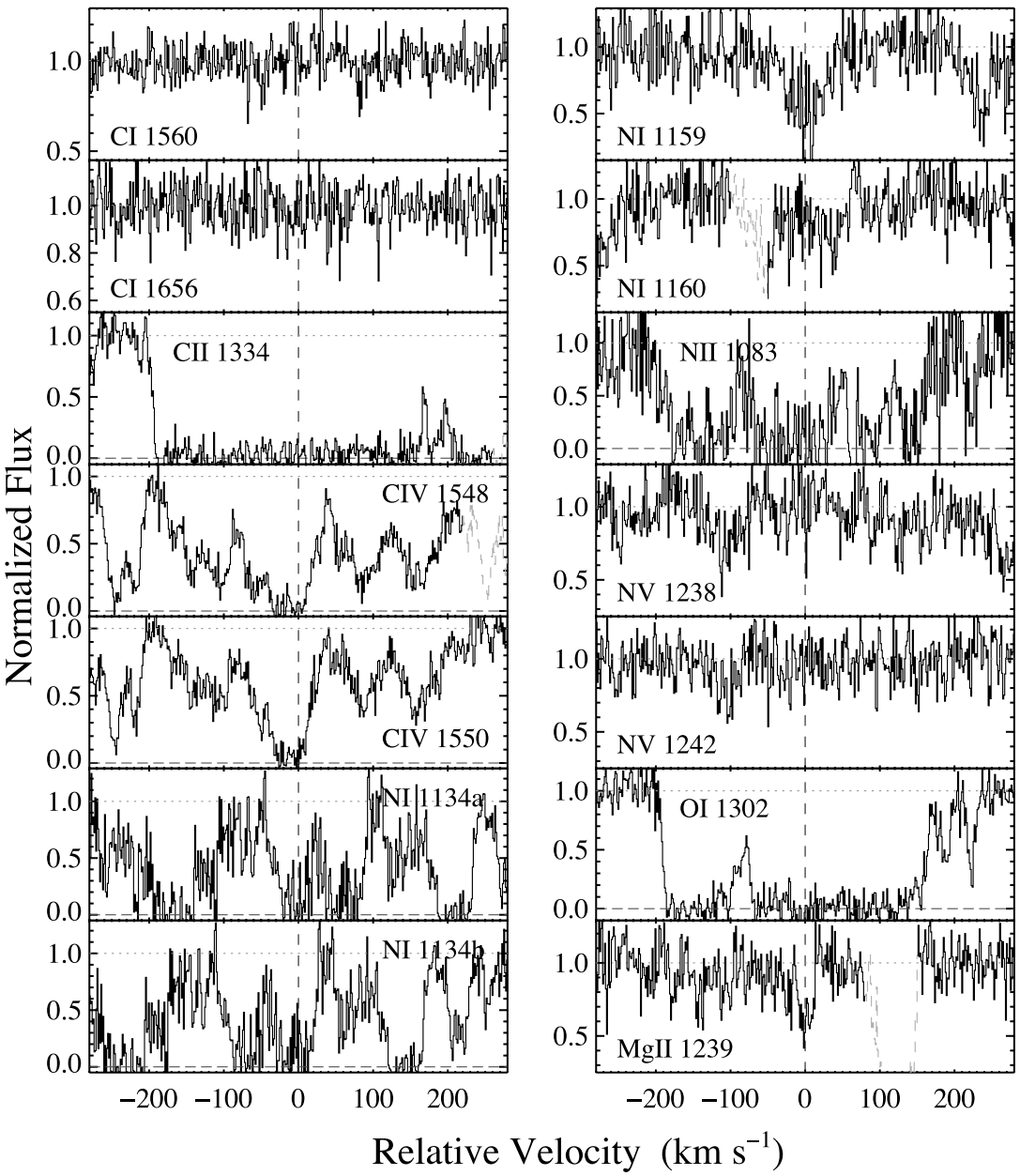

FIG. 5.—Velocity profiles of the resonance transitions identified in the ISM of the host galaxy of GRB 050820. The velocity $v = 0$ km s^{-1} corresponds to $z = 2.61469$. The profiles are ordered by atomic number and ionization state. [*See the electronic edition of the Supplement for a color version of this figure.*]

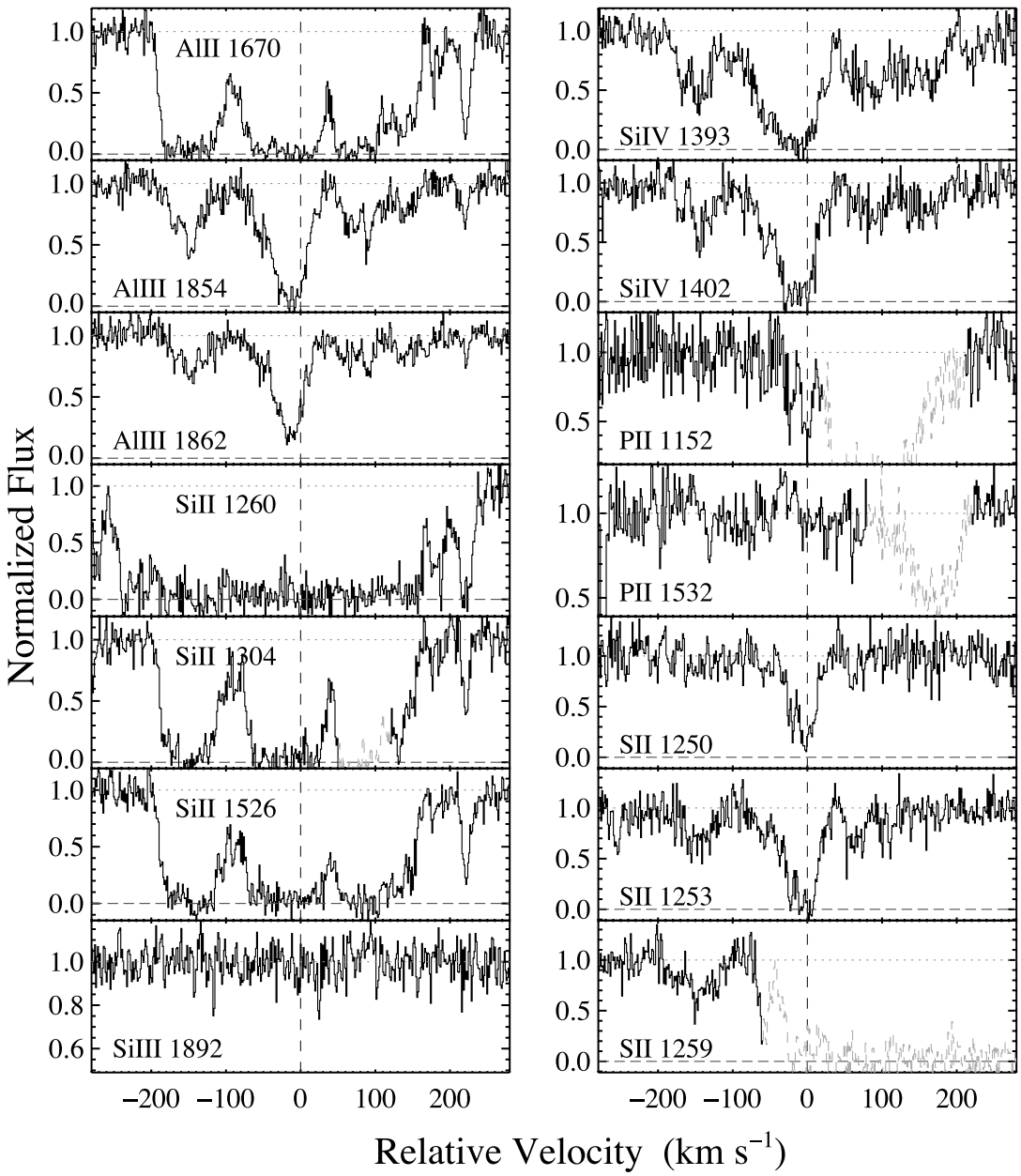

FIG. 5—*Continued*

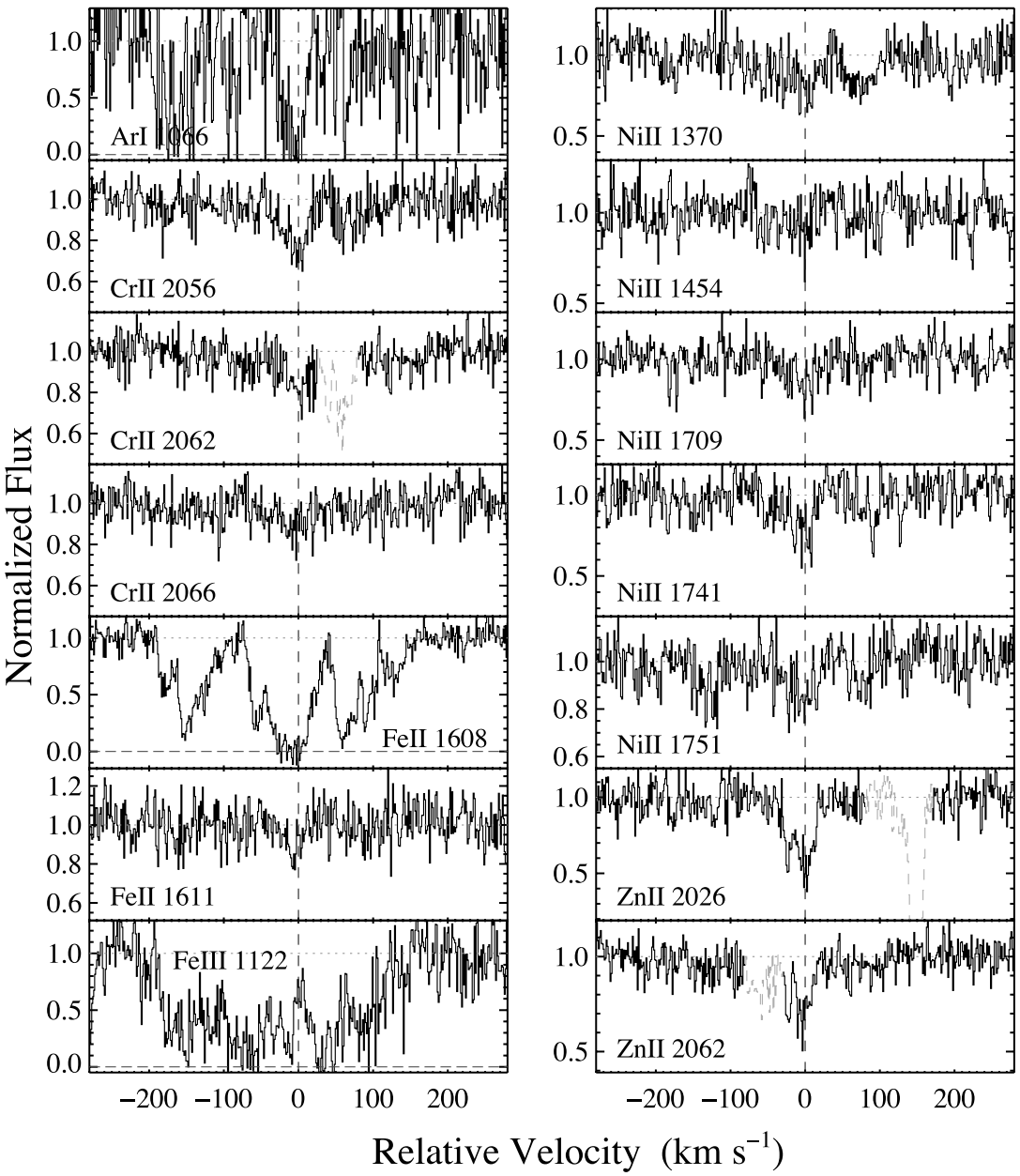

FIG. 5—*Continued*

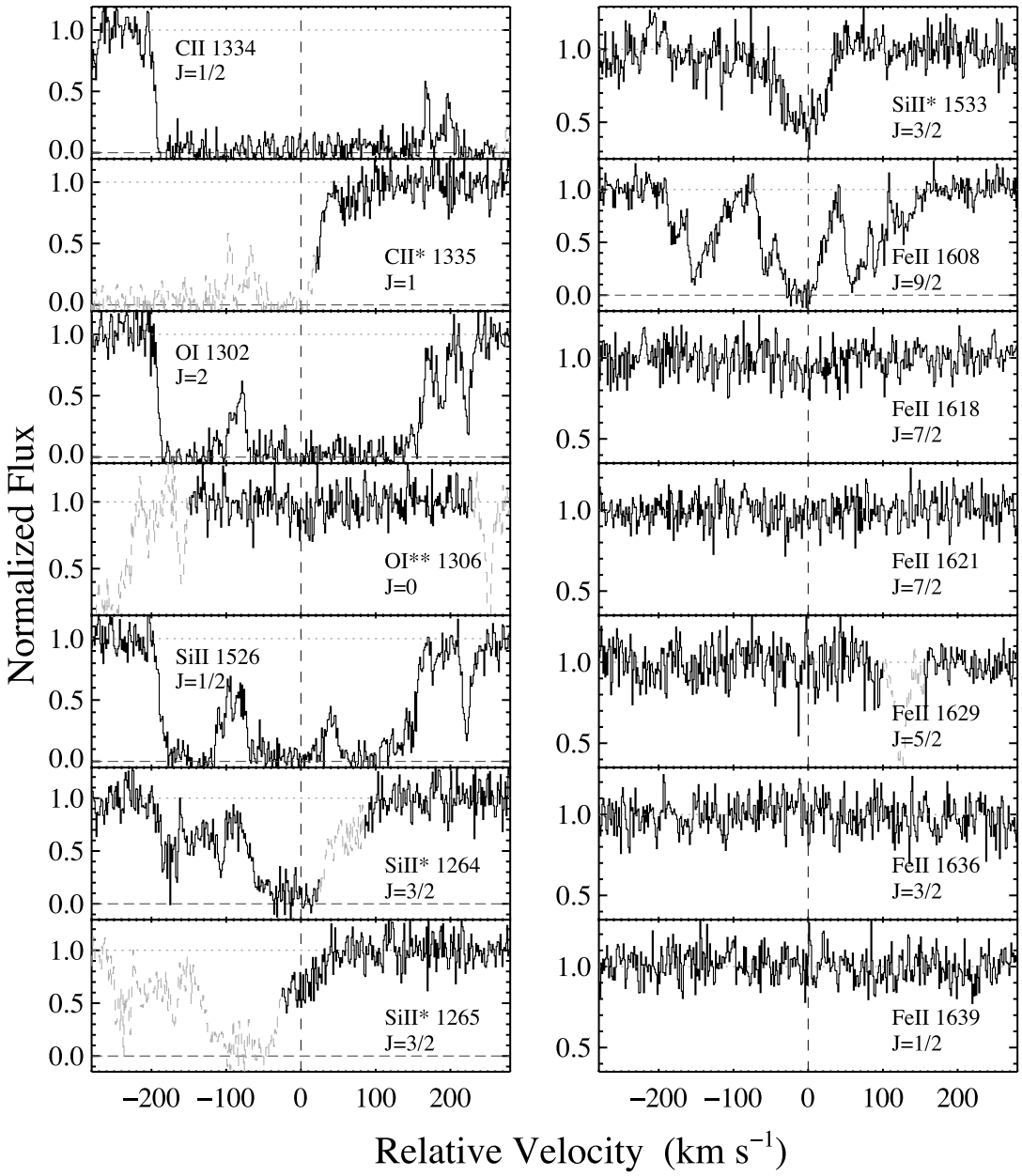

FIG. 6.—Velocity profiles of the fine-structure transitions (with several resonance lines for comparison) identified in the ISM of the host galaxy of GRB 050820. The velocity $v = 0$ km s^{-1} corresponds to $z = 2.61469$. The profiles are ordered by atomic number and energy level. [*See the electronic edition of the Supplement for a color version of this figure.*]

4.2. *GRB 050820*

The *Swift* BAT instrument triggered on GRB 050820 at UT 2005 August 20 06:34:53 and the *Swift* team issued an XRT position within a few minutes (Page et al. 2005). Fox & Cenko (2005) reported a bright ($R \sim 14.7$), optical afterglow at R.A. = $22^{\rm h}29^{\rm m}38.11^{\rm s}$, decl. = $+19^\circ33'37.1''$. We began acquiring data with the HIRES echelle spectrometer on the Keck I telescope shortly after. Our instrumental configuration followed the standard setup for the UC planet hunters (e.g., Vogt et al. 2005). The short slit length ($3''$) complicated sky-subtraction, although the seeing ($0.7''$) was sufficiently good to give fair results.

In Figure 4, we present the echelle orders covering the Lyα profile for the host galaxy of GRB 050820. Overplotted is a fit to the data that yields $\log N_{\rm H\,II} = 21.0 \pm 0.1$dex. The uncertainty in this fit is dominated by continuum error, which is related to difficulties in fluxing this echelle data.

Figure 5 shows the velocity profiles for the resonance lines associated with the ISM of the host galaxy. Figure 6 shows the fine-structure transitions and a resonance line for comparison. Finally, Table 3 lists the column density measurements for all of the transitions.

4.3. *GRB 051111*

The *Swift* BAT instrument triggered on GRB 051111 at UT 2005 November 11 05:59:39 (Yamaoka et al. 2005). Owing to the moon constraint, XRT observations were delayed until 5000 s after the trigger (La Parola et al. 2005). Rujopakarn et al. (2005) reported an optical afterglow at R.A. = $23^{\rm h}12^{\rm m}33.2^{\rm s}$, decl. = $+18^\circ22'29.1''$. Although Keck I was scheduled for engineering on this night, the observatory kindly agreed to switch instruments to HIRES and obtain echelle spectroscopy of GRB 050820 (Hill et al. 2005).

TABLE 3

IONIC COLUMN DENSITIES FOR HG 050820

Ion	J[a]	E_J (cm^{-1})	λ (Å)	log f	$v_{\rm int}$[b] (km s^{-1})	W_λ[c] (mÅ)	log N	log $N_{\rm adopt}$
C I	0	0.00	1277.2450	−1.0148	[−40, 40]	<12.1	<13.13	<12.75
	0	0.00	1560.3092	−1.0947	[−40, 40]	<10.7	<12.96	
	0	0.00	1656.9283	−0.8523	[−30, 50]	<12.3	<12.75	
C II	1/2	0.00	1334.5323	−0.8935	[−220, 280]	2047.3 ± 9.4	>15.54	>15.54
	3/2	63.40	1335.7077	−0.9397	[40, 100]	30.3 ± 4.4	13.28 ± 0.06	13.28 ± 0.06
C IV		0.00	1548.1950	−0.7194	[−300, 200]	1505.3 ± 10.4	>14.88	>15.00
		0.00	1550.7700	−1.0213	[−300, 200]	1138.6 ± 12.1	>15.00	
N I		0.00	1159.8170	−5.0701	[−50, 50]	<16.4	<18.26	<18.26
		0.00	1160.9370	−5.6198	[−50, 50]	<14.6	<18.60	
N II	1/2	0.00	1083.9900	−0.9867	[−250, 200]	1084.8 ± 24.7	>15.36	>15.36
N V		0.00	1238.8210	−0.8041	[−50, 50]	<13.9	<13.00	<13.00
		0.00	1242.8040	−1.1066	[−40, 80]	<15.1	<13.35	
O I	2	0.00	1302.1685	−1.3110	[−210, 280]	1562.1 ± 10.9	>15.84	>15.84
	0	226.98	1306.0286	−1.3122	[−50, 50]	<10.9	<13.41	<13.41
Mg I		0.00	1827.9351	−1.6216	[−40, 40]	<10.9	<13.37	<12.60
		0.00	2026.4768	−0.9508	[−20, 40]	<10.7	<12.60	
Mg II		0.00	1239.9253	−3.1986	[−40, 40]	48.1 ± 5.9	15.86 ± 0.05	15.86 ± 0.05
		0.00	1240.3947	−3.4498	[−40, 40]	<10.2	<17.13	
Al II		0.00	1670.7874	0.2742	[−220, 280]	1810.8 ± 9.9	>14.09	>14.09
Al III		0.00	1854.7164	−0.2684	[−220, 280]	698.9 ± 11.9	>13.88	13.90 ± 0.01
		0.00	1862.7895	−0.5719	[−220, 280]	458.5 ± 11.8	13.90 ± 0.01	
Si I		0.00	1845.5200	−0.6402	[−40, 40]	<12.4	<12.44	<12.44
Si II	1/2	0.00	1260.4221	0.0030	[−210, 280]	1703.3 ± 12.2	>14.57	>15.43
	1/2	0.00	1304.3702	−1.0269	[−210, 280]	1280.7 ± 10.4	>15.43	
	1/2	0.00	1526.7066	−0.8962	[−220, 280]	1646.9 ± 11.3	>15.28	
	3/2	287.24	1264.7377	−0.0441	[−210, 120]	673.5 ± 10.6	>14.05	13.73 ± 0.02
	3/2	287.24	1265.0020	−0.9983	[−20, 40]	<9.3	<13.83	
	3/2	287.24	1533.4312	−0.6396	[−190, 20]	198.6 ± 8.3	13.73 ± 0.02	
	3/2	287.24	1817.4512	−3.8894	[−40, 40]	<10.9	<15.64	
Si III		0.00	1892.0300	−4.5702	[−40, 40]	<9.5	<16.24	<16.24
Si IV		0.00	1393.7550	−0.2774	[−200, 200]	817.7 ± 10.7	>14.23	>14.34
		0.00	1402.7700	−0.5817	[−220, 200]	521.6 ± 12.1	>14.34	
P II	1/2	0.00	1152.8180	−0.6271	[−80, 30]	86.6 ± 8.0	13.64 ± 0.04	13.64 ± 0.04
	1/2	0.00	1532.5330	−2.1186	[−60, 60]	<13.4	<14.12	
S II		0.00	1250.5840	−2.2634	[−210, 140]	163.4 ± 13.1	15.57 ± 0.04	15.57 ± 0.04
		0.00	1253.8110	−1.9634	[−210, 140]	364.6 ± 12.0	>15.67	
Ar I		0.00	1066.6600	−1.1709	[−50, 50]	135.1 ± 15.7	>14.61	>14.61
Cr II		0.00	2056.2539	−0.9788	[−50, 50]	69.8 ± 5.5	13.31 ± 0.03	13.33 ± 0.02
		0.00	2062.2340	−1.1079	[−50, 30]	59.3 ± 5.1	13.35 ± 0.04	
		0.00	2066.1610	−1.2882	[−40, 40]	41.9 ± 5.6	13.37 ± 0.06	
Fe II	9/2	0.00	1608.4511	−1.2366	[−200, 150]	895.5 ± 9.5	>15.15	14.82 ± 0.12
	9/2	0.00	1611.2005	−2.8665	[−80, 10]	17.9 ± 5.4	14.82 ± 0.12	
	7/2	384.79	1618.4680	−1.6696	[−30, 30]	<9.2	<13.66	<13.31
	7/2	384.79	1621.6856	−1.4191	[−30, 30]	<8.6	<13.31	
	5/2	667.68	1629.1596	−1.4353	[−30, 30]	<10.9	<13.29	<13.29
	3/2	862.61	1634.3498	−1.6882	[−30, 30]	<9.2	<13.46	<13.15
	3/2	862.61	1636.3313	−1.3925	[−30, 30]	<9.3	<13.15	
	1/2	977.05	1639.4012	−1.2373	[−30, 30]	<8.7	<12.97	<12.97
Ni II		0.00	1370.1310	−1.1141	[−90, 100]	<16.2	<13.96	13.69 ± 0.04
		0.00	1703.4050	−2.2218	[−50, 50]	<11.0	<14.04	
		0.00	1709.6042	−1.4895	[−50, 50]	37.0 ± 5.9	13.70 ± 0.07	
		0.00	1741.5490	−1.3696	[−40, 40]	43.6 ± 5.5	13.66 ± 0.05	
		0.00	1751.9157	−1.5575	[−50, 50]	35.5 ± 5.8	13.73 ± 0.07	
Zn II		0.00	2026.1360	−0.3107	[−50, 50]	124.3 ± 6.5	12.95 ± 0.02	12.96 ± 0.02
		0.00	2062.6640	−0.5918	[−30, 50]	78.3 ± 5.0	12.98 ± 0.03	

[a] Total angular momentum of the electron spin and orbital angular moment. The quantity E_J is the energy above the ground state.
[b] Velocity interval over which the equivalent width and column density are measured.
[c] Rest equivalent width.

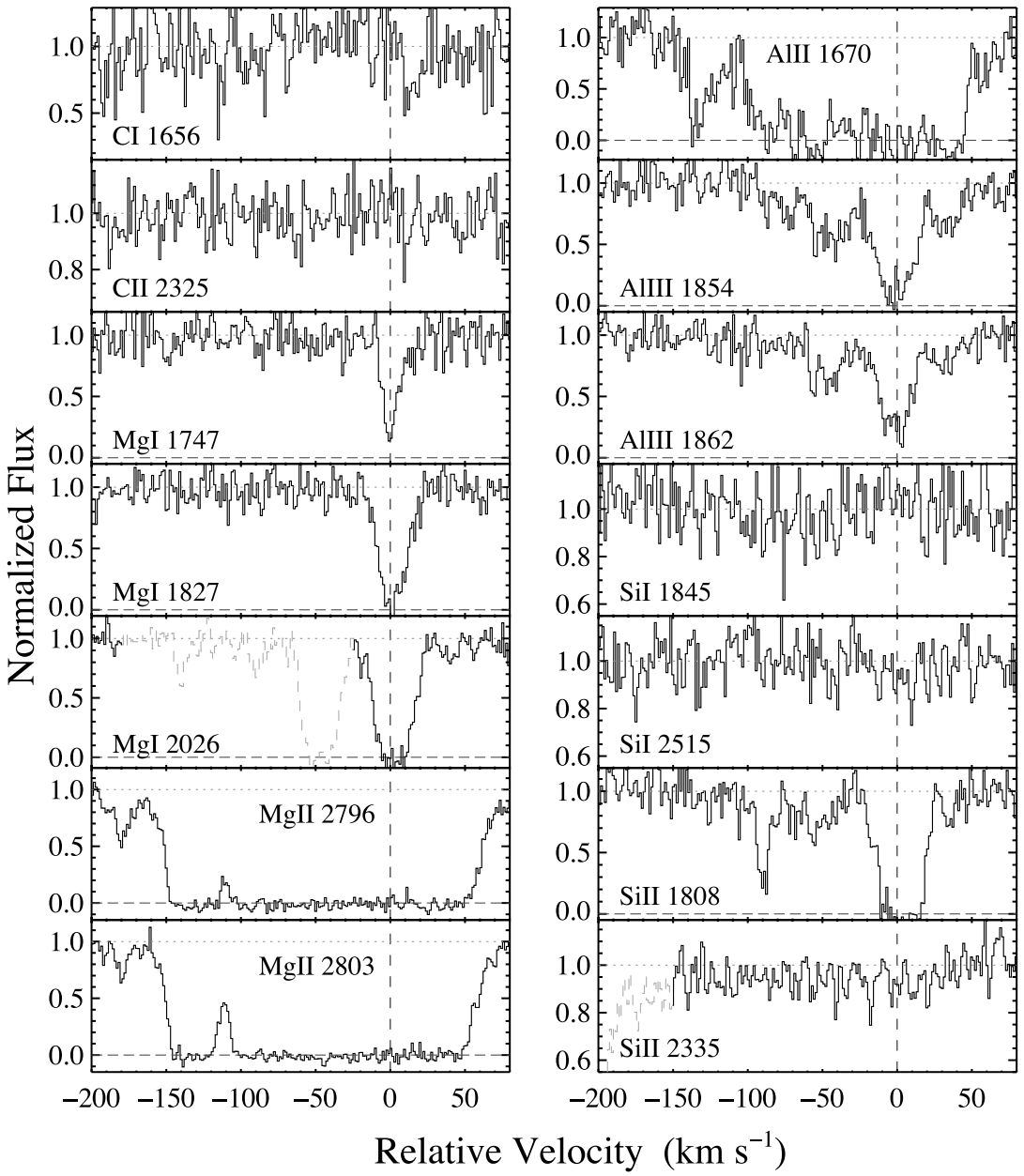

FIG. 7.—Velocity profiles of the resonance transitions identified in the ISM of the host galaxy of GRB 051111. The velocity $v = 0$ km s^{-1} corresponds to $z = 1.54948$. The profiles are ordered by atomic number and ionization state. [*See the electronic edition of the Supplement for a color version of this figure.*]

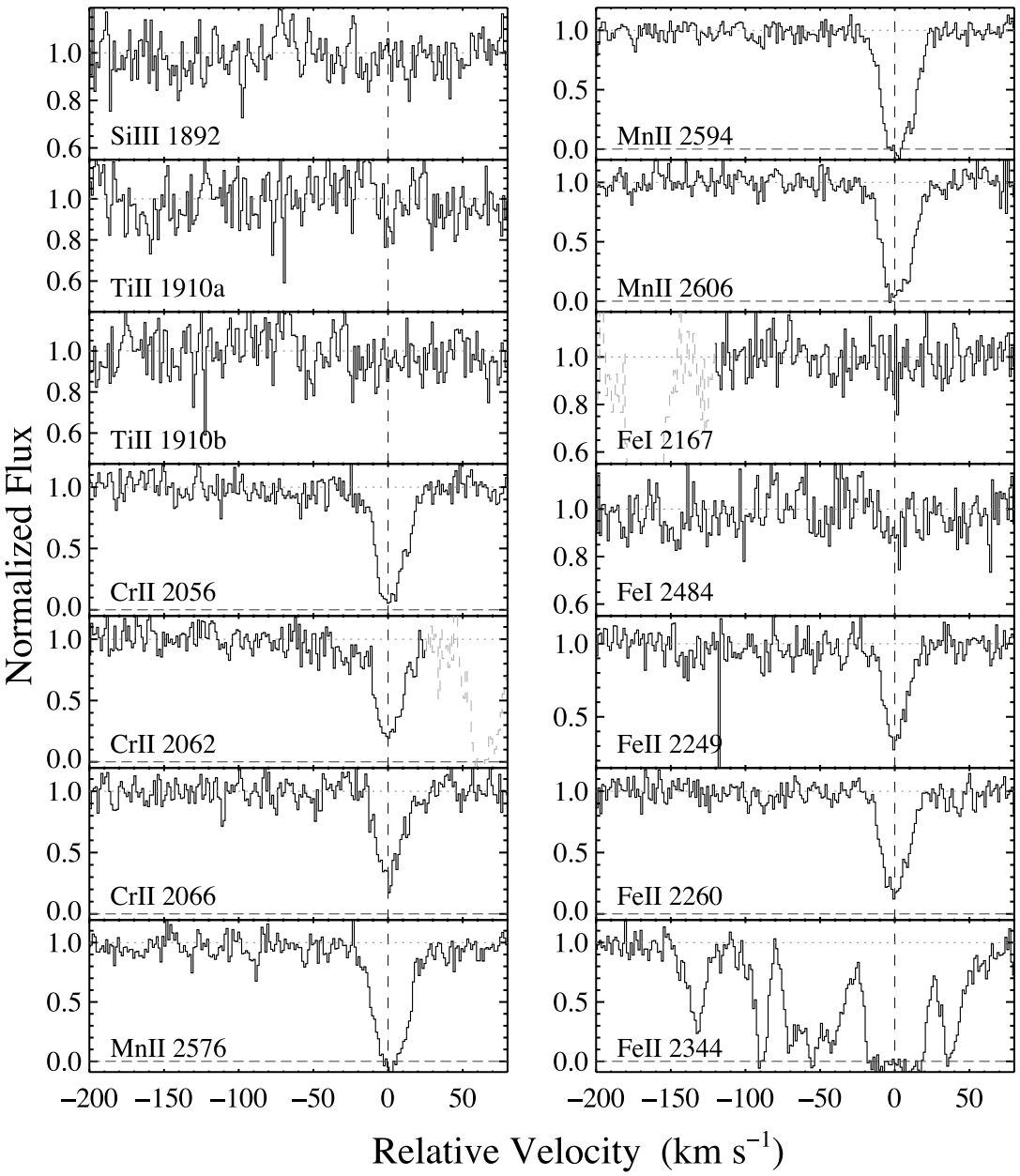

FIG. 7—*Continued*

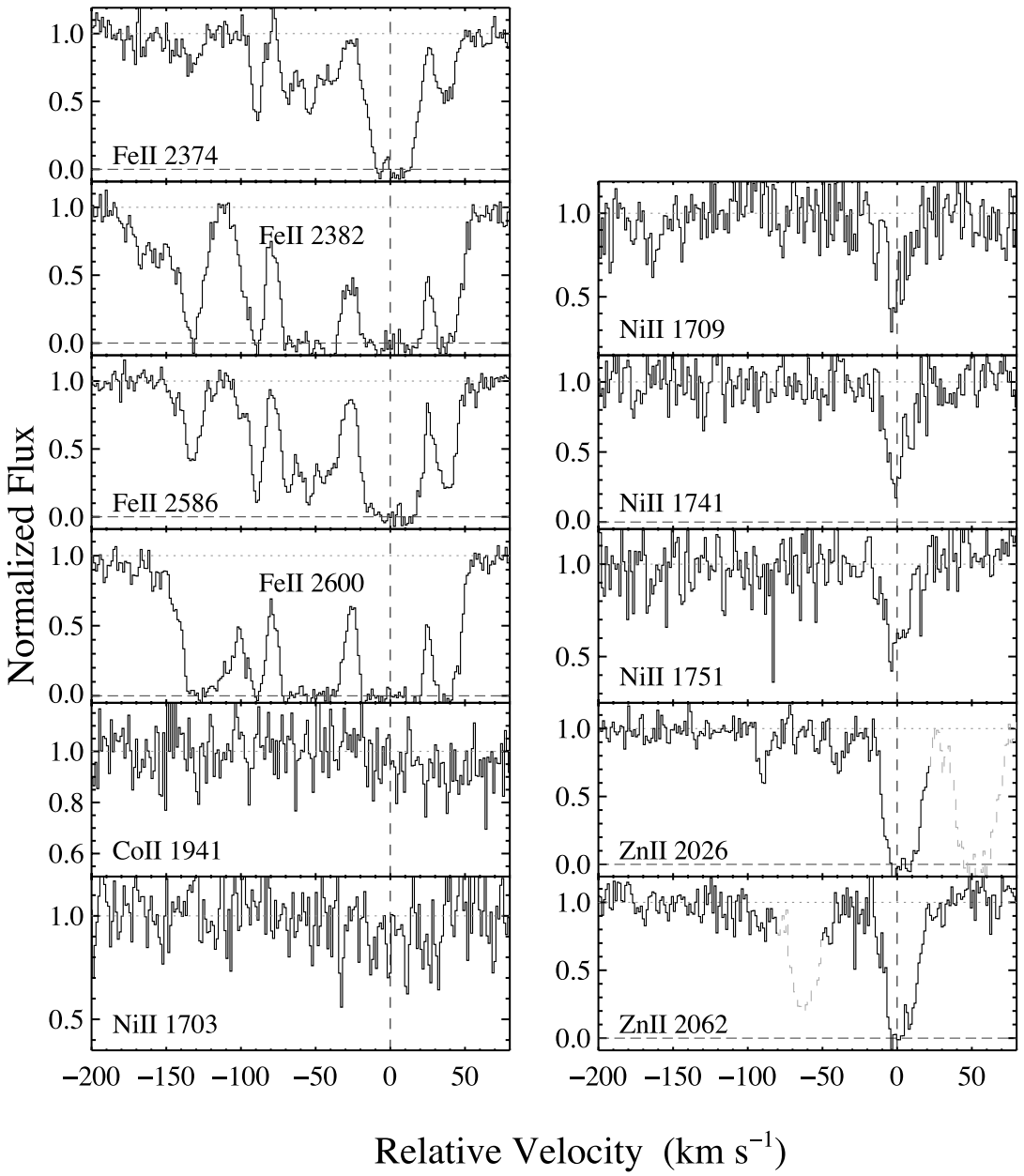

FIG. 7—*Continued*

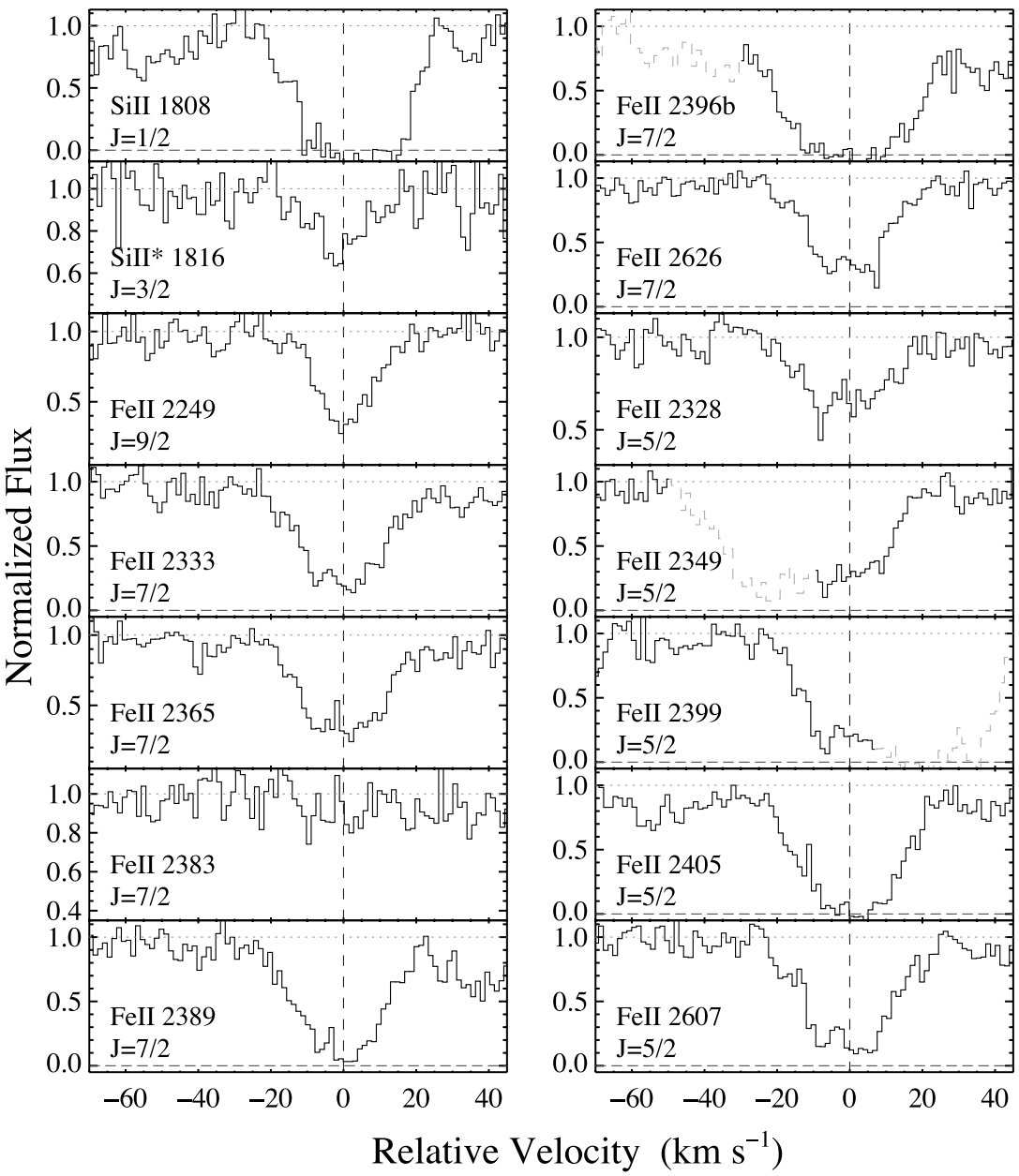

FIG. 8.—Velocity profiles of the fine-structure transitions (with several resonance lines for comparison) identified in the ISM of the host galaxy of GRB 051111. The velocity $v = 0$ km s^{-1} corresponds to $z = 1.54948$. The profiles are ordered by atomic number and energy level. [*See the electronic edition of the Supplement for a color version of this figure.*]

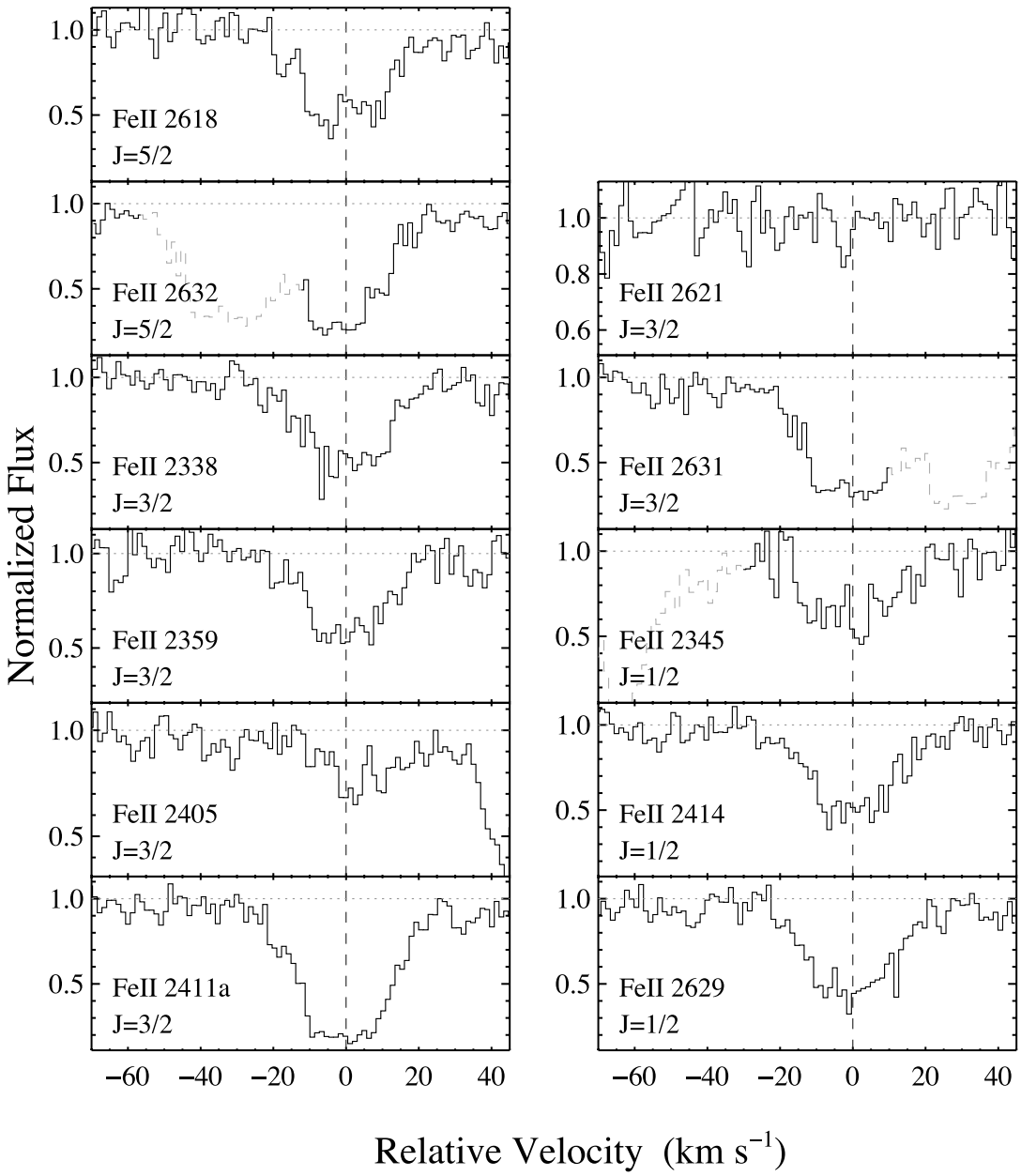

FIG. 8—*Continued*

TABLE 4

IONIC COLUMN DENSITIES FOR HG 051111

Ion	J[a]	E_J (cm^{-1})	λ (Å)	log f	v_{int}[b] ($km\ s^{-1}$)	W_λ[c] (mÅ)	log N	log N_{adopt}
C I	0	0.00	1656.9283	−0.8523	[−40, 40]	<20.6	<12.99	<12.99
C II	1/2	0.00	2325.4030	−7.3484	[−40, 40]	<10.0	<18.85	<18.84
Mg I		0.00	1747.7937	−2.0419	[−40, 40]	72.3 ± 6.1	14.68 ± 0.04	14.68 ± 0.04
		0.00	1827.9351	−1.6216	[−40, 40]	133.3 ± 5.9	>14.63	
		0.00	2026.4768	−0.9508	[−40, 40]	279.7 ± 4.3	>14.31	
Mg II		0.00	2796.3520	−0.2130	[−200, 70]	2102.1 ± 6.3	>14.35	>14.62
		0.00	2803.5310	−0.5151	[−200, 70]	1994.4 ± 6.7	>14.62	
Al II		0.00	1670.7874	0.2742	[−180, 80]	945.5 ± 14.0	>13.75	>13.75
Al III		0.00	1854.7164	−0.2684	[−130, 40]	331.1 ± 8.7	>13.57	13.63 ± 0.02
		0.00	1862.7895	−0.5719	[−130, 40]	245.3 ± 7.8	13.63 ± 0.02	
Si I		0.00	1845.5200	−0.6402	[−40, 40]	<12.2	<12.42	<12.42
		0.00	2515.0730	−0.7905	[−40, 40]	<12.3	<12.43	
Si II	1/2	0.00	1808.0130	−2.6603	[−100, 40]	338.4 ± 7.8	>16.14	>16.14
	1/2	0.00	2335.1230	−5.3716	[−40, 40]	<9.3	<17.32	
	3/2	287.24	1816.9285	−2.7799	[−40, 40]	42.2 ± 6.3	15.00 ± 0.06	15.00 ± 0.06
Si III		0.00	1892.0300	−4.5702	[−40, 40]	<11.1	<16.32	<16.32
Ti II	1/2	0.00	1910.6000	−0.6946	[−40, 40]	<11.4	<12.42	<12.42
Cr II		0.00	2056.2539	−0.9788	[−40, 40]	154.9 ± 5.1	13.90 ± 0.03	13.88 ± 0.01
		0.00	2062.2340	−1.1079	[−40, 40]	149.4 ± 5.4	13.89 ± 0.02	
		0.00	2066.1610	−1.2882	[−40, 40]	88.8 ± 5.5	13.85 ± 0.03	
Mn II		0.00	2576.8770	−0.4549	[−40, 40]	260.6 ± 5.1	>13.55	>13.64
		0.00	2594.4990	−0.5670	[−40, 40]	229.5 ± 4.1	>13.64	
		0.00	2606.4620	−0.7151	[−40, 40]	213.2 ± 5.3	>13.64	
Fe I		0.00	2484.0210	−0.2541	[−40, 40]	<11.3	<11.75	<11.76
Fe II	9/2	0.00	2249.8768	−2.7397	[−100, 40]	112.9 ± 6.8	15.28 ± 0.02	15.32 ± 0.01
	9/2	0.00	2260.7805	−2.6126	[−120, 40]	155.1 ± 6.5	15.35 ± 0.02	
	9/2	0.00	2344.2140	−0.9431	[−200, 80]	985.6 ± 9.5	>14.70	
	9/2	0.00	2374.4612	−1.5045	[−180, 80]	569.0 ± 7.9	>14.96	
	9/2	0.00	2382.7650	−0.4949	[−200, 80]	1313.9 ± 8.6	>14.43	
	9/2	0.00	2586.6499	−1.1605	[−180, 100]	916.4 ± 7.9	>14.76	
	9/2	0.00	2600.1729	−0.6216	[−200, 100]	1523.8 ± 7.8	>14.59	
	7/2	384.79	2333.5160	−1.1601	[−40, 40]	205.9 ± 4.3	13.99 ± 0.01	14.01 ± 0.01
	7/2	384.79	2365.5520	−1.3054	[−40, 40]	178.8 ± 4.7	14.02 ± 0.01	
	7/2	384.79	2383.7884	−2.2861	[−40, 40]	30.1 ± 5.8	14.12 ± 0.08	
	7/2	384.79	2389.3582	−1.0835	[−40, 20]	216.9 ± 5.3	>14.08	
	7/2	384.79	2396.3559	−0.5414	[−40, 40]	405.8 ± 4.9	>13.90	
	7/2	384.79	2626.4511	−1.3556	[−40, 40]	182.3 ± 5.2	14.01 ± 0.01	
	5/2	667.68	2328.1110	−1.4492	[−40, 40]	85.6 ± 4.6	13.78 ± 0.02	13.78 ± 0.01
	5/2	667.68	2607.8664	−0.9281	[−40, 40]	232.3 ± 5.5	13.78 ± 0.02	
	5/2	667.68	2618.3991	−1.2967	[−40, 40]	140.1 ± 5.8	13.78 ± 0.02	
	3/2	862.61	2338.7250	−1.0339	[−40, 40]	126.8 ± 4.8	13.57 ± 0.02	13.59 ± 0.01
	3/2	862.61	2359.8280	−1.2421	[−40, 40]	98.6 ± 5.2	13.64 ± 0.02	
	3/2	862.61	2621.1912	−2.4067	[−40, 40]	<11.5	<13.86	
	1/2	977.05	2345.0010	−0.8027	[−25, 40]	97.9 ± 5.3	13.20 ± 0.03	13.26 ± 0.01
	1/2	977.05	2414.0450	−0.7557	[−40, 40]	126.5 ± 4.4	13.26 ± 0.02	
	1/2	977.05	2622.4518	−1.2518	[−40, 40]	61.0 ± 5.7	13.31 ± 0.04	
	1/2	977.05	2629.0777	−0.7620	[−40, 40]	156.3 ± 4.9	13.29 ± 0.02	
Co II		0.00	1941.2852	−1.4685	[−40, 40]	<10.3	<13.16	<13.16
Ni II		0.00	1703.4050	−2.2218	[−40, 40]	<14.6	<14.46	13.97 ± 0.03
		0.00	1709.6042	−1.4895	[−40, 40]	54.2 ± 7.2	13.96 ± 0.05	
		0.00	1741.5531	−1.3696	[−40, 40]	76.6 ± 6.8	14.00 ± 0.04	
		0.00	1751.9157	−1.5575	[−40, 40]	48.5 ± 6.8	13.93 ± 0.06	
Zn II		0.00	2026.1360	−0.3107	[−40, 40]	237.9 ± 4.4	>13.60	>13.71
		0.00	2062.6640	−0.5918	[−40, 40]	176.7 ± 5.0	>13.71	

[a] Total angular momentum of the electron spin and orbital angular moment. The quantity E_J is the energy above the ground state.
[b] Velocity interval over which the equivalent width and column density are measured.
[c] Rest equivalent width.

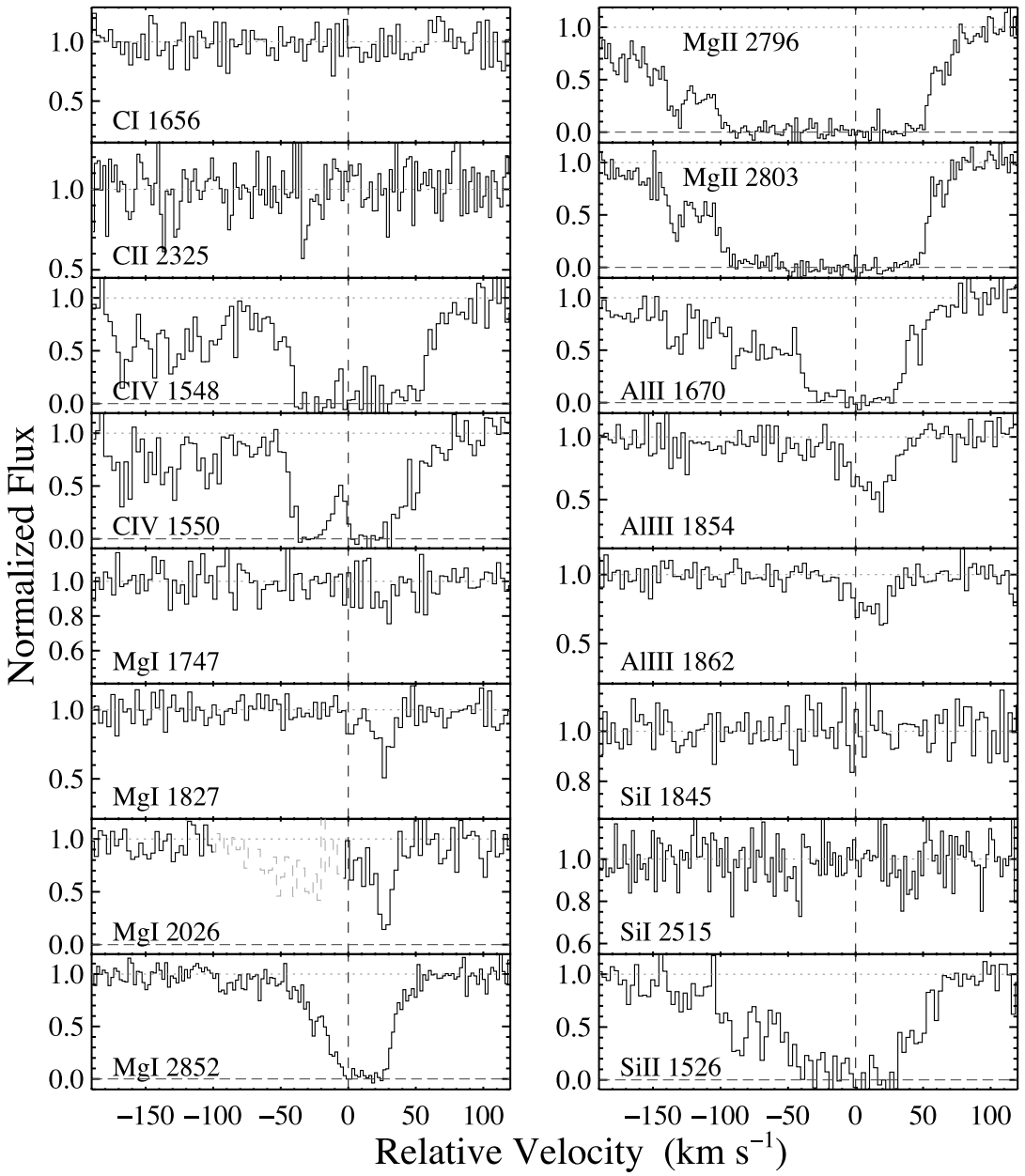

FIG. 9.—Velocity profiles of the resonance transitions identified in the ISM of the host galaxy of GRB 060418. The velocity $v = 0$ km s^{-1} corresponds to $z = 1.490$. The profiles are ordered by atomic number and ionization state. [*See the electronic edition of the Supplement for a color version of this figure.*]

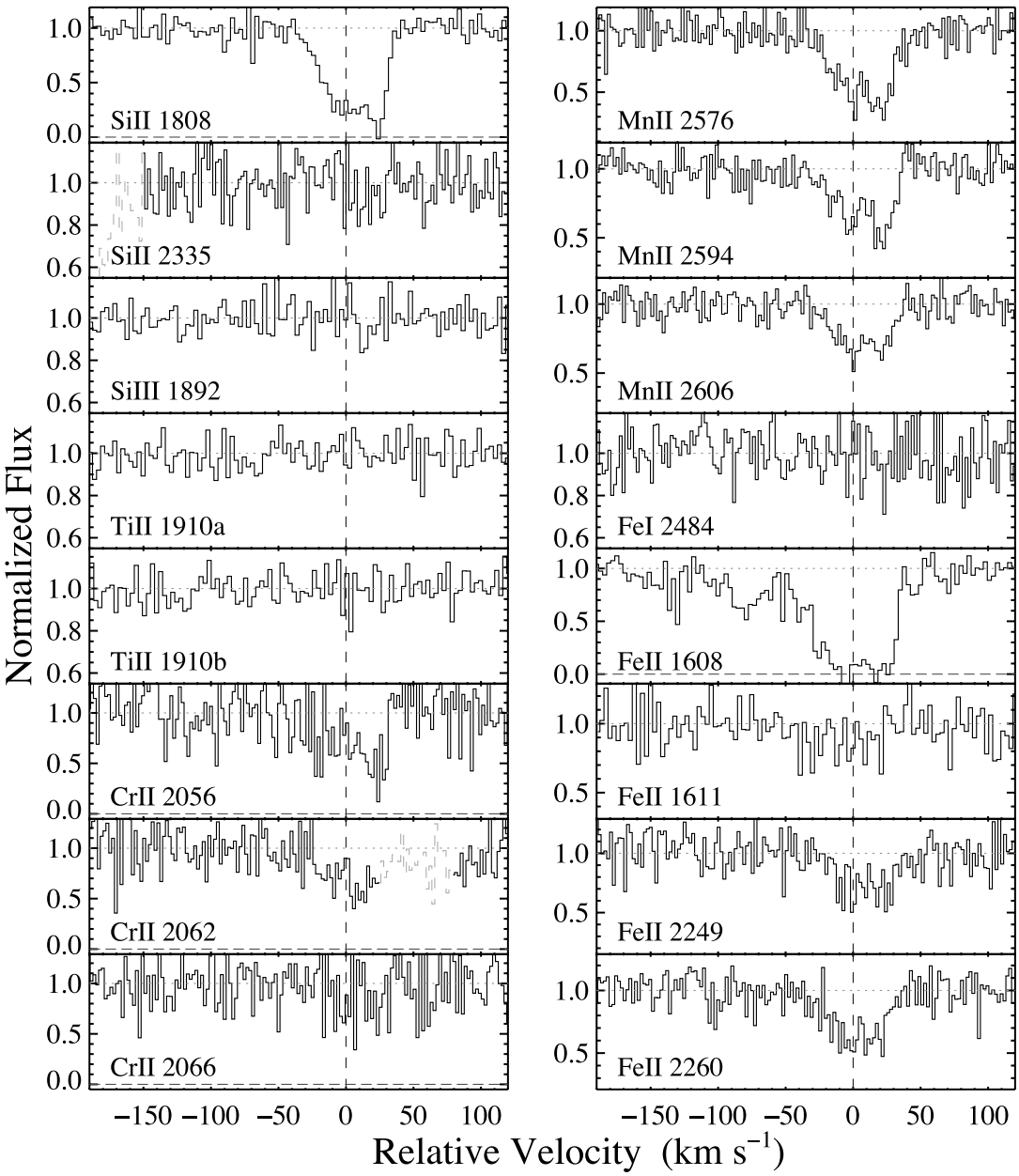

FIG. 9—*Continued*

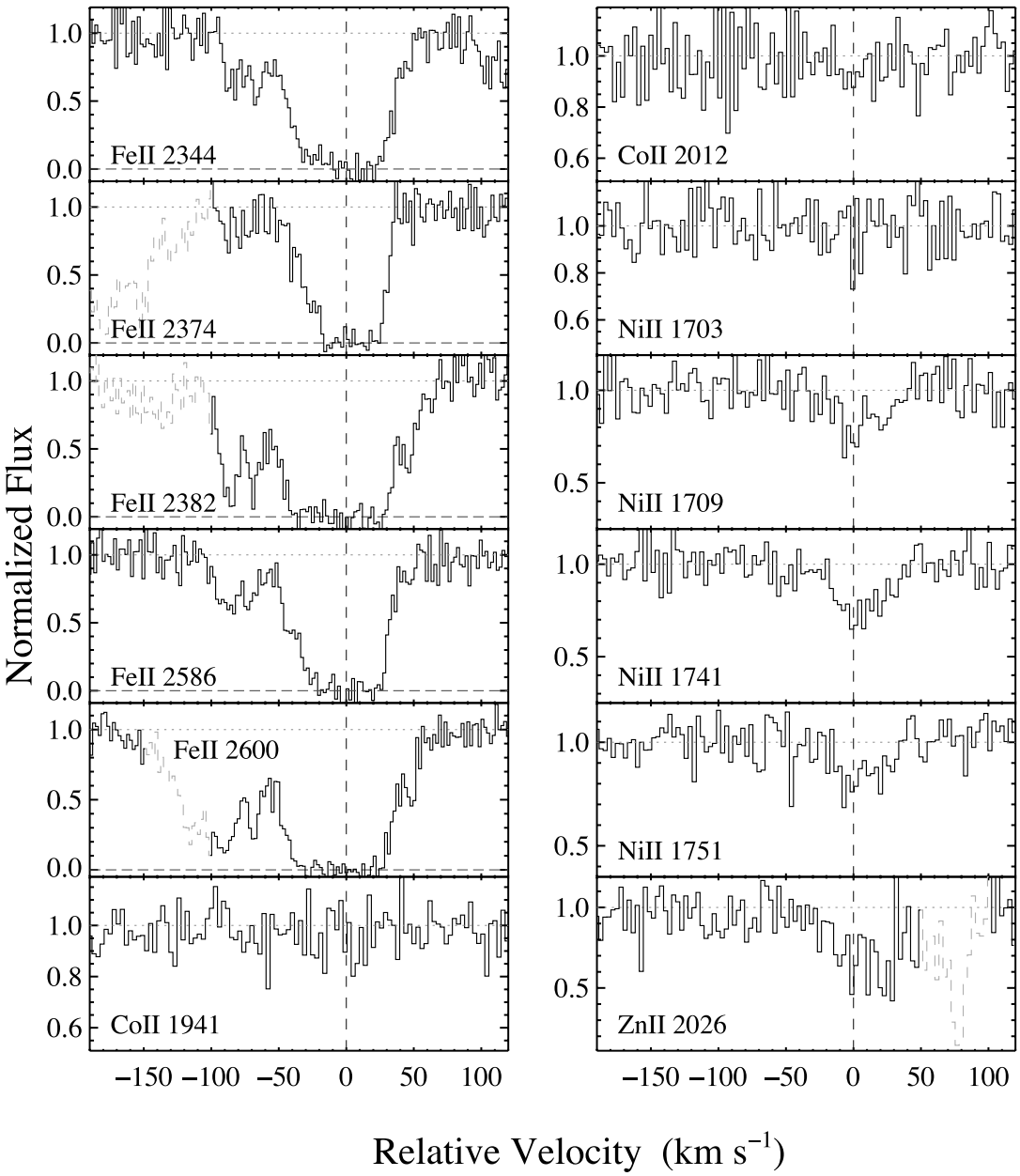

FIG. 9—*Continued*

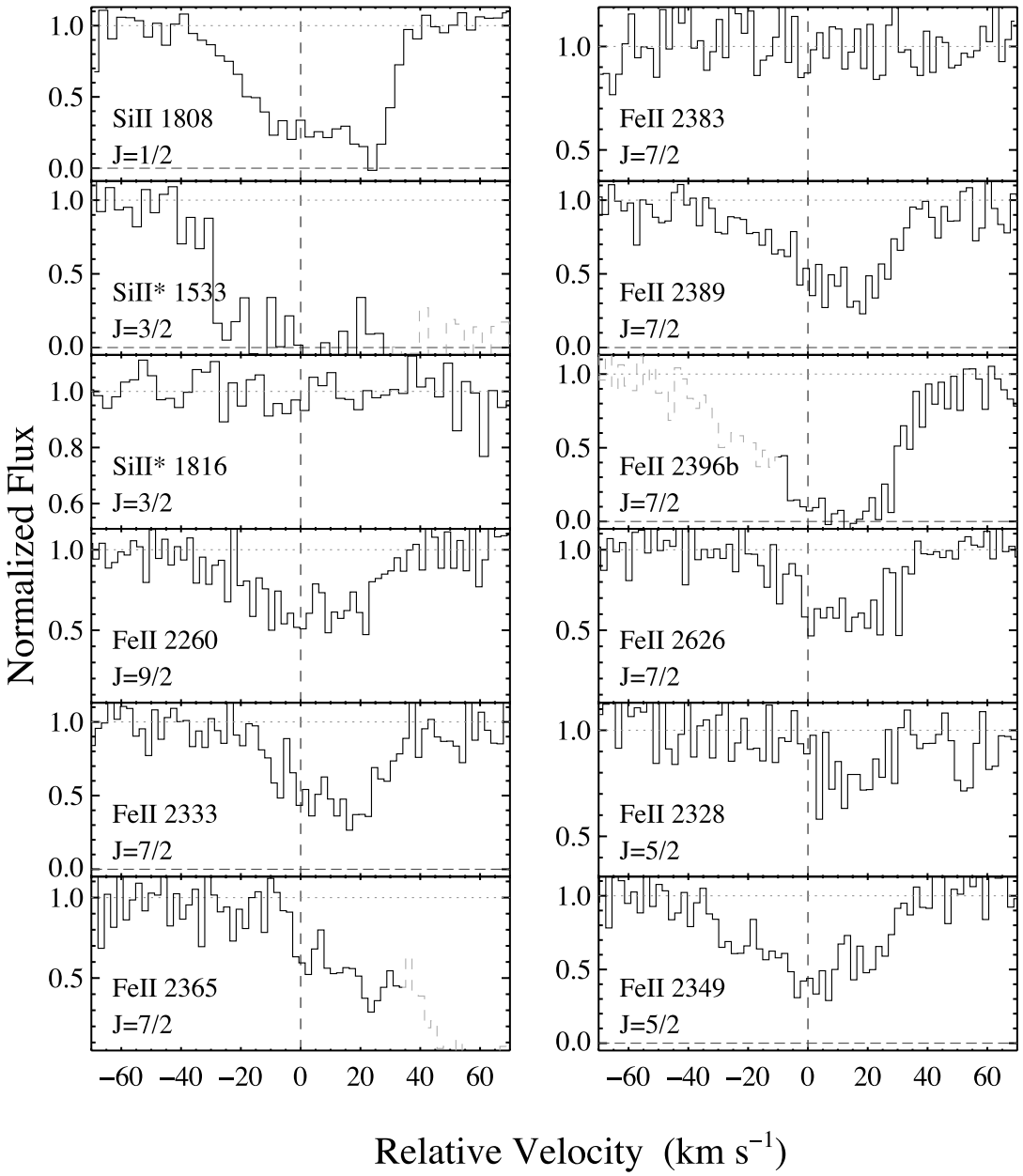

FIG. 10.—Velocity profiles of the fine-structure transitions (with several resonance lines for comparison) identified in the ISM of the host galaxy of GRB 060418. The velocity $v = 0$ km s^{-1} corresponds to $z = 1.490$. The profiles are ordered by atomic number and energy level. [*See the electronic edition of the Supplement for a color version of this figure.*]

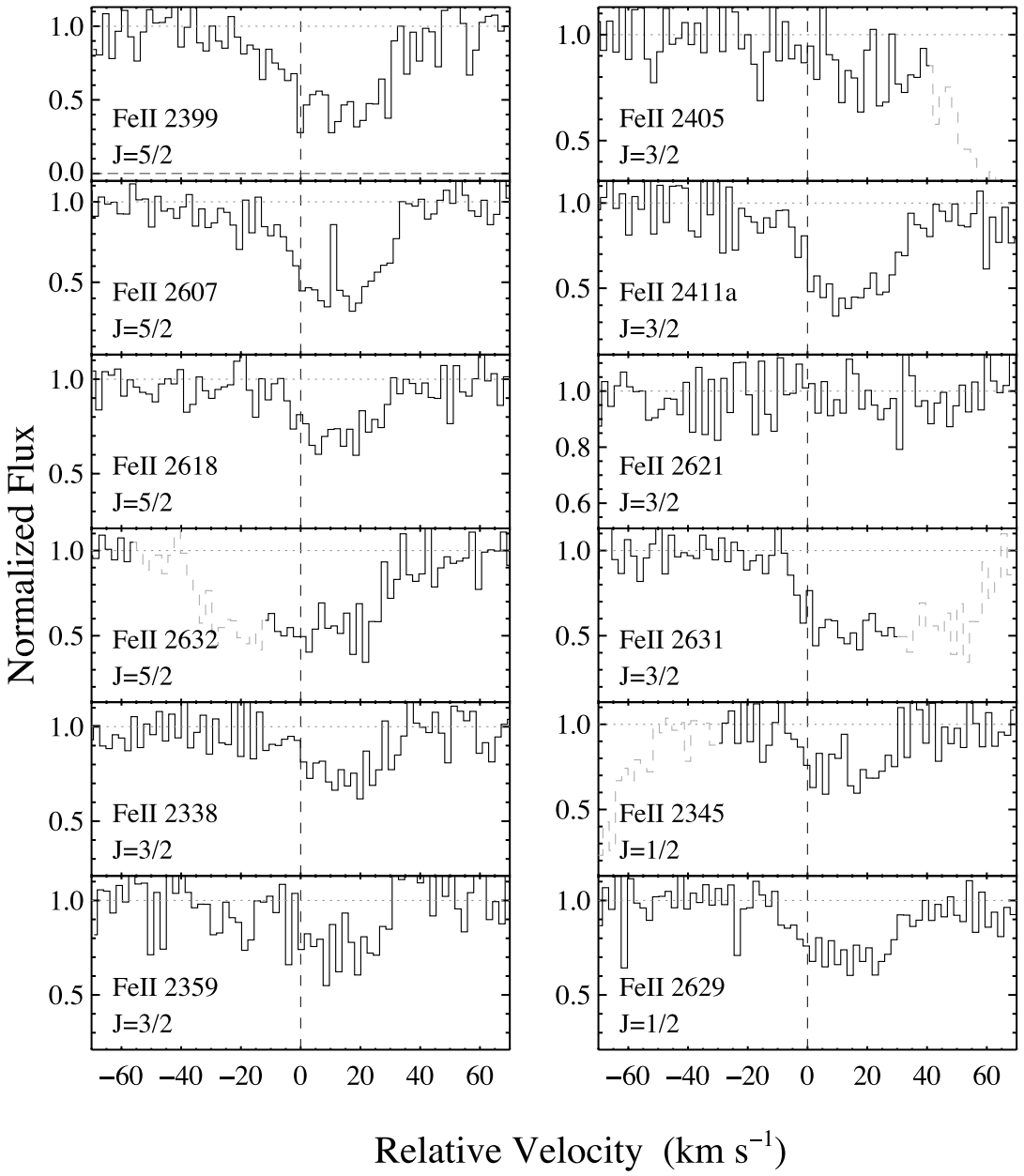

FIG. 10—*Continued*

TABLE 5

IONIC COLUMN DENSITIES FOR HG 060418

Ion	J[a]	E_J (cm^{-1})	λ (Å)	log f	v_{int}[b] ($km\ s^{-1}$)	W_λ[c] (mÅ)	log N	log N_{adopt}
C I	0	0.00	1656.9283	−0.8523	[−50, 50]	<18.2	<12.93	<12.93
C II	1/2	0.00	2325.4030	−7.3484	[−50, 50]	<26.7	<19.28	<19.28
C IV		0.00	1548.1950	−0.7194	[−190, 110]	802.9 ± 19.1	>14.68	>14.88
		0.00	1550.7700	−1.0213	[−190, 110]	610.5 ± 17.7	>14.88	
Mg I		0.00	1747.7937	−2.0419	[−40, 40]	<12.7	<13.91	13.70 ± 0.05
		0.00	1827.9351	−1.6216	[−20, 50]	40.8 ± 6.5	13.84 ± 0.06	
		0.00	2026.4768	−0.9508	[0, 50]	109.1 ± 10.9	13.63 ± 0.06	
		0.00	2852.9642	0.2577	[−100, 80]	597.8 ± 11.3	>13.12	
Mg II		0.00	2796.3520	−0.2130	[−200, 100]	1927.7 ± 13.4	>14.20	>14.46
		0.00	2803.5310	−0.5151	[−200, 100]	1694.5 ± 13.3	>14.46	
Al II		0.00	1670.7874	0.2742	[−180, 80]	718.0 ± 11.8	>13.59	>13.59
Al III		0.00	1854.7164	−0.2684	[−50, 50]	122.2 ± 6.7	12.97 ± 0.03	12.95 ± 0.02
		0.00	1862.7895	−0.5719	[−50, 50]	56.2 ± 6.8	12.90 ± 0.05	
Si I		0.00	1845.5200	−0.6402	[−40, 40]	<12.6	<12.44	<12.44
		0.00	2515.0730	−0.7905	[−40, 40]	<17.8	<12.48	
Si II	1/2	0.00	1526.7066	−0.8962	[−190, 110]	659.0 ± 18.6	>14.76	>15.89
	1/2	0.00	1808.0130	−2.6603	[−50, 50]	252.0 ± 6.5	>15.89	
	1/2	0.00	2335.1230	−5.3716	[−40, 40]	<21.0	<17.19	
	3/2	287.24	1533.4312	−0.6396	[−50, 30]	304.7 ± 9.8	>14.26	>14.26
	3/2	287.24	1816.9285	−2.7799	[−40, 40]	<12.7	<14.60	
Si III		0.00	1892.0300	−4.5702	[−40, 40]	<12.0	<16.33	<16.33
Ti II	1/2	0.00	1910.6000	−0.6946	[−40, 40]	<11.5	<12.42	<12.42
Cr II		0.00	2056.2539	−0.9788	[−50, 50]	127.5 ± 17.0	13.72 ± 0.07	13.71 ± 0.04
		0.00	2062.2340	−1.1079	[−50, 50]	135.9 ± 15.8	13.77 ± 0.05	
		0.00	2066.1610	−1.2882	[−40, 40]	<30.4	13.53 ± 0.13	
Mn II		0.00	2576.8770	−0.4549	[−50, 50]	247.2 ± 9.9	13.23 ± 0.02	13.16 ± 0.01
		0.00	2594.4990	−0.5670	[−50, 50]	162.1 ± 9.8	13.11 ± 0.03	
		0.00	2606.4620	−0.7151	[−50, 50]	133.9 ± 9.1	13.14 ± 0.03	
Co II		0.00	1941.2852	−1.4685	[−40, 40]	<12.9	<13.25	<13.25
Fe I		0.00	2484.0210	−0.2541	[−40, 40]	<20.5	<12.02	<12.02
Fe II	9/2	0.00	1608.4511	−1.2366	[−120, 70]	446.0 ± 11.5	>14.92	15.22 ± 0.03
	9/2	0.00	1611.2005	−2.8665	[−50, 50]	45.4 ± 9.3	15.25 ± 0.08	
	9/2	0.00	2249.8768	−2.7397	[−50, 50]	110.8 ± 13.0	15.23 ± 0.05	
	9/2	0.00	2260.7805	−2.6126	[−50, 50]	142.4 ± 10.8	15.21 ± 0.03	
	9/2	0.00	2344.2140	−0.9431	[−120, 80]	729.4 ± 14.4	>14.57	
	9/2	0.00	2374.4612	−1.5045	[−100, 80]	546.6 ± 13.3	>15.04	
	9/2	0.00	2382.7650	−0.4949	[−100, 80]	987.1 ± 11.2	>14.27	
	9/2	0.00	2586.6499	−1.1605	[−130, 70]	779.0 ± 13.5	>14.74	
	9/2	0.00	2600.1729	−0.6216	[−100, 100]	1075.3 ± 10.7	>14.38	
	7/2	384.79	2333.5160	−1.1601	[−40, 45]	184.8 ± 10.1	13.89 ± 0.03	13.88 ± 0.02
	7/2	384.79	2383.7884	−2.2861	[−40, 40]	<19.9	<14.06	
	7/2	384.79	2389.3582	−1.0835	[−50, 50]	232.1 ± 10.4	13.90 ± 0.02	
	7/2	384.79	2396.3559	−0.5414	[−80, 80]	432.7 ± 14.1	>13.85	
	7/2	384.79	2626.4511	−1.3556	[−40, 50]	143.5 ± 9.7	13.84 ± 0.03	
	5/2	667.68	2328.1110	−1.4492	[−40, 50]	58.2 ± 12.0	13.61 ± 0.08	13.63 ± 0.01
	5/2	667.68	2349.0220	−1.0841	[−60, 60]	211.1 ± 11.8	13.86 ± 0.03	
	5/2	667.68	2399.9728	−0.9255	[−40, 50]	198.7 ± 11.1	13.67 ± 0.03	
	5/2	667.68	2607.8664	−0.9281	[−40, 40]	193.3 ± 8.2	13.57 ± 0.02	
	5/2	667.68	2618.3991	−1.2967	[−40, 40]	95.7 ± 8.7	13.57 ± 0.04	
	3/2	862.61	2338.7250	−1.0339	[−30, 40]	69.2 ± 9.1	13.26 ± 0.06	13.33 ± 0.02
	3/2	862.61	2359.8280	−1.2421	[−40, 40]	65.7 ± 11.5	13.46 ± 0.07	
	3/2	862.61	2411.2533	−0.6778	[−40, 40]	173.1 ± 9.9	13.34 ± 0.03	
	3/2	862.61	2621.1912	−2.4067	[−40, 40]	<18.7	<14.08	
	1/2	977.05	2345.0010	−0.8027	[−25, 40]	70.8 ± 8.8	13.05 ± 0.05	13.05 ± 0.03
	1/2	977.05	2414.0450	−0.7557	[−40, 40]	305.7 ± 8.4	>13.93	
	1/2	977.05	2622.4518	−1.2518	[−40, 40]	28.5 ± 9.3	12.98 ± 0.13	
	1/2	977.05	2629.0777	−0.7620	[−40, 50]	104.7 ± 9.9	13.07 ± 0.04	
Ni II		0.00	1703.4050	−2.2218	[−40, 40]	<13.1	<14.12	13.84 ± 0.03
		0.00	1709.6042	−1.4895	[−40, 40]	50.4 ± 6.6	13.83 ± 0.06	
		0.00	1741.5531	−1.3696	[−50, 50]	70.8 ± 7.4	13.85 ± 0.05	
		0.00	1751.9157	−1.5575	[−40, 40]	43.9 ± 6.6	13.81 ± 0.06	
Zn II		0.00	2026.1360	−0.3107	[−50, 50]	147.7 ± 14.9	13.03 ± 0.05	13.02 ± 0.04
		0.00	2062.6640	−0.5918	[−40, 25]	79.2 ± 12.8	13.00 ± 0.07	

[a] Total angular momentum of the electron spin and orbital angular moment. The quantity E_J is the energy above the ground state.
[b] Velocity interval over which the equivalent width and column density are measured.
[c] Rest equivalent width.

TABLE 6

SUMMARY TABLE FOR THE ISM IN GRB HOST GALAXIES

Parameter	HG 050730	HG 050820	HG 051111	HG 060418
z	3.9686	2.6147	1.5495	1.4900
$\log N_{\rm H\,II}$	$22.15^{+0.10}_{-0.10}$	$21.00^{+0.10}_{-0.10}$	23.00	23.00
[M/H][a]	−2.26	−0.63	>−2.78	>−2.65
$\log N(\rm Fe^+)$[b]	15.15	14.90	15.36	15.26
[C/Fe]	>−1.04	>−0.45	...	...
[N/Fe]	−0.85	<+2.89	...	...
[O/Fe]	>−0.89	>−0.30	...	...
[Mg/Fe]	<+0.85	+0.88	>−0.83	>−0.88
[Al/Fe]	>−0.60	>+0.20	>−0.61	>−0.66
[Si/Fe]	>−0.28	>+0.48	>+0.75	>+0.58
[P/Fe]	<+1.04	+0.71	...	...
[S/Fe]	+0.24	+0.97	...	...
[Ti/Fe]	...	...	<−0.39	<−0.27
[Cr/Fe]	...	+0.26	+0.35	+0.28
[Mn/Fe]	...	...	>+0.25	−0.12
[Co/Fe]	...	...	<+0.38	<+0.58
[Ni/Fe]	−0.22	+0.04	−0.15	−0.17
[Zn/Fe]	...	+0.89	>+1.18	+0.59
$\log N(\rm O^0)_{J=1}$	>14.94			
$\log N(\rm O^0)_{J=0}$	>14.61	<13.41		
$\log N(\rm Si^+)_{J=3/2}$	>14.56	13.73 ± 0.02	15.00 ± 0.06	>14.26
$\log N(\rm Fe^+)_{J=7/2}$	14.29 ± 0.04	<13.31	14.01 ± 0.01	13.88 ± 0.02
$\log N(\rm Fe^+)_{J=5/2}$	14.12 ± 0.07	<13.29	13.78 ± 0.01	13.63 ± 0.01
$\log N(\rm Fe^+)_{J=3/2}$	13.92 ± 0.06	<13.15	13.59 ± 0.01	13.33 ± 0.02
$\log N(\rm Fe^+)_{J=1/2}$	13.65 ± 0.07	<12.97	13.26 ± 0.01	13.05 ± 0.03
$\log N(\rm Mg^0)$		<12.60	14.68 ± 0.04	13.70 ± 0.05

NOTES.—We assume the solar abundance measurements given by Asplund et al. (2005) throughout this table. Furthermore, we do not adopt ionization corrections or differential depletion corrections.

[a] Metallicity based on S, Si, and Zn in that order of preference. Lower limits assume $N_{\rm H\,II} = 10^{23}$ cm^{-2}.

[b] Corrected for the population of the excited levels for this and all of the following entries.

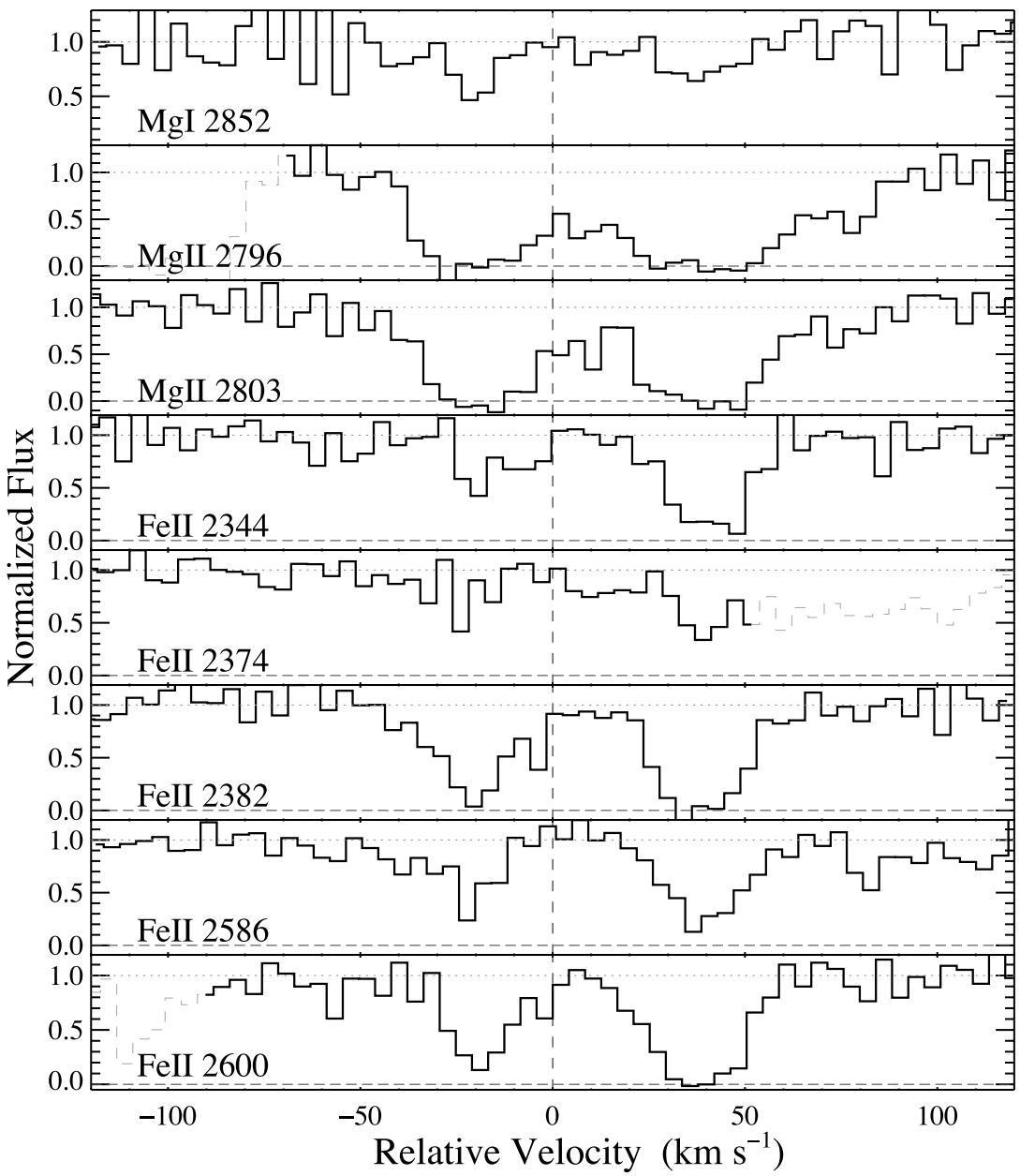

FIG. 11.—Velocity profiles of the transitions identified with the Mg II absorber at $z = 1.773$ toward GRB 050730. [*See the electronic edition of the Supplement for a color version of this figure.*]

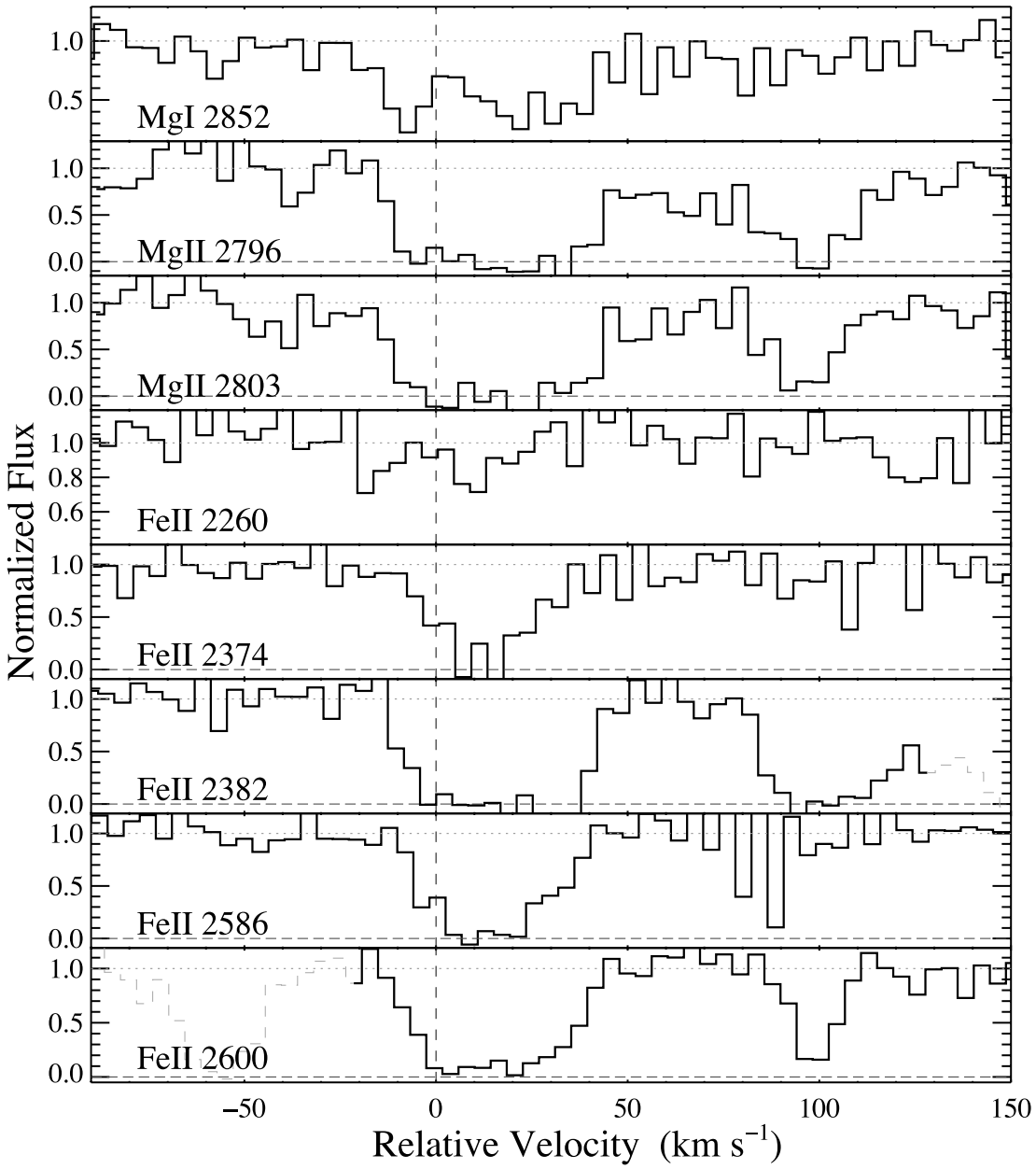

FIG. 12.—Velocity profiles of the transitions identified with the Mg II absorber at $z = 2.253$ toward GRB 050730. [*See the electronic edition of the Supplement for a color version of this figure.*]

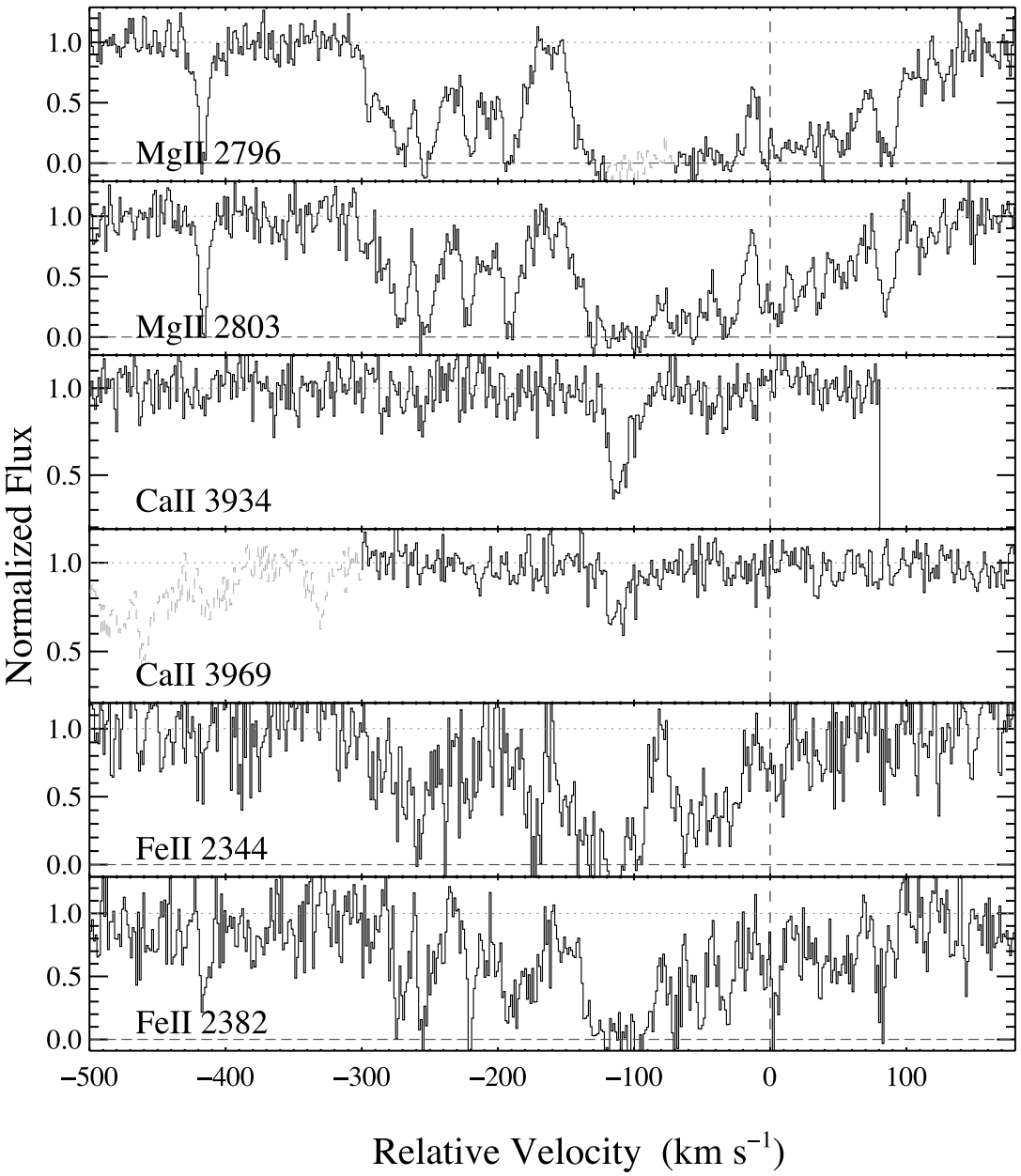

FIG. 13.—Velocity profiles of the transitions identified with the Mg II absorber at $z = 0.692$ toward GRB 050820. [*See the electronic edition of the Supplement for a color version of this figure.*]

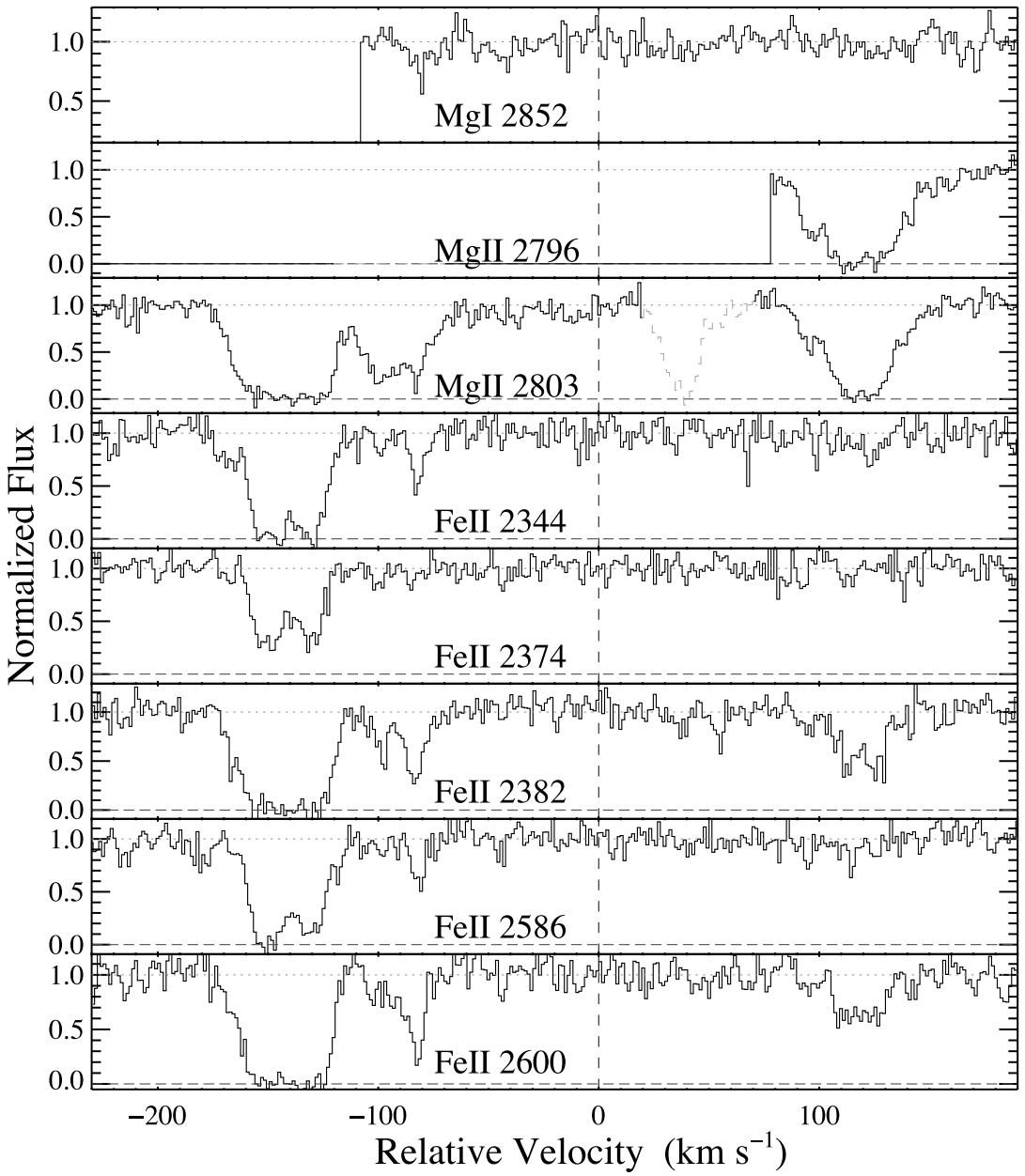

FIG. 14.—Velocity profiles of the transitions identified with the Mg II absorber at $z = 1.430$ toward GRB 050820. [*See the electronic edition of the Supplement for a color version of this figure.*]

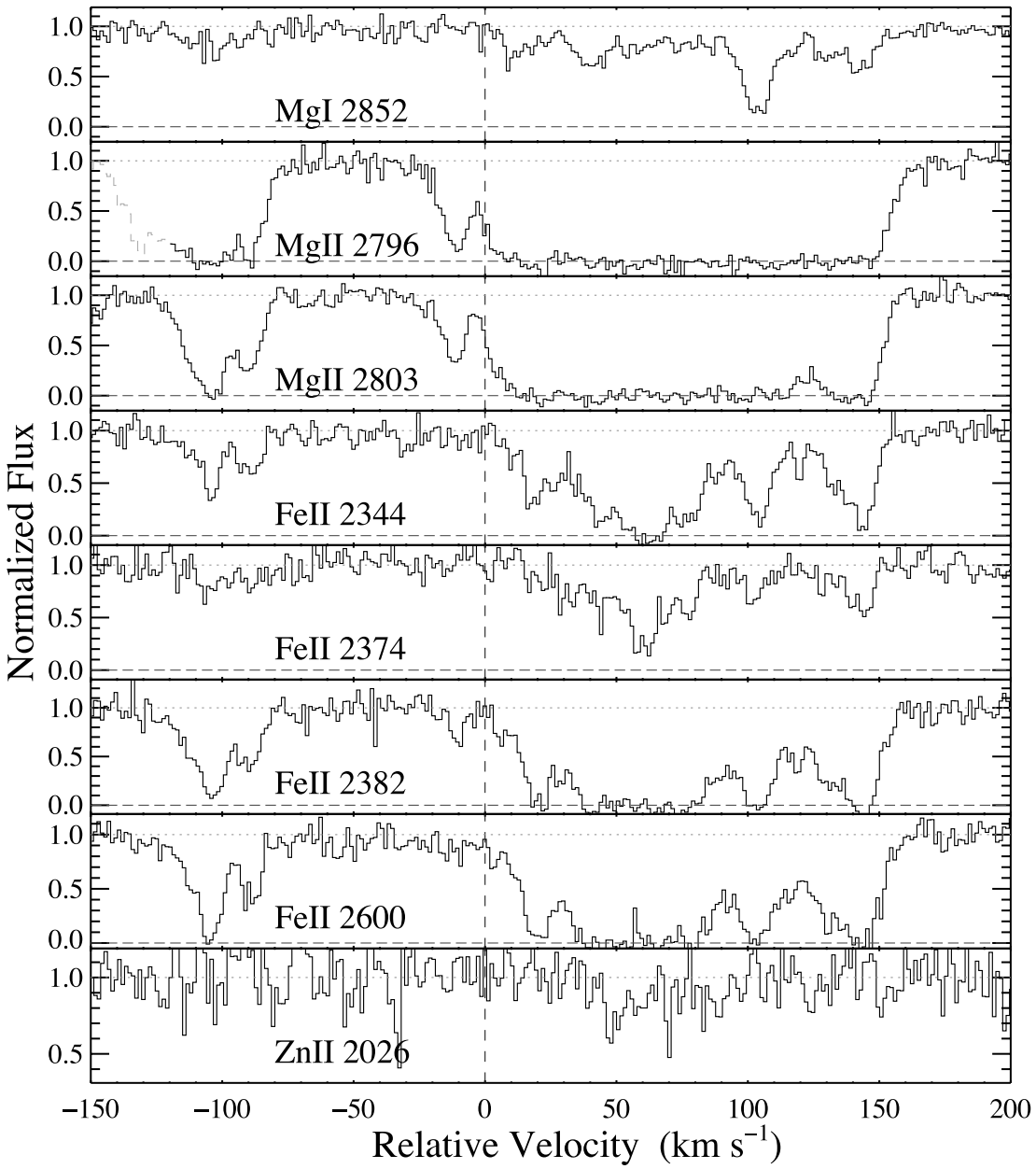

FIG. 15.—Velocity profiles of the transitions identified with the Mg II absorber at $z = 1.189$ toward GRB 051111. [*See the electronic edition of the Supplement for a color version of this figure.*]

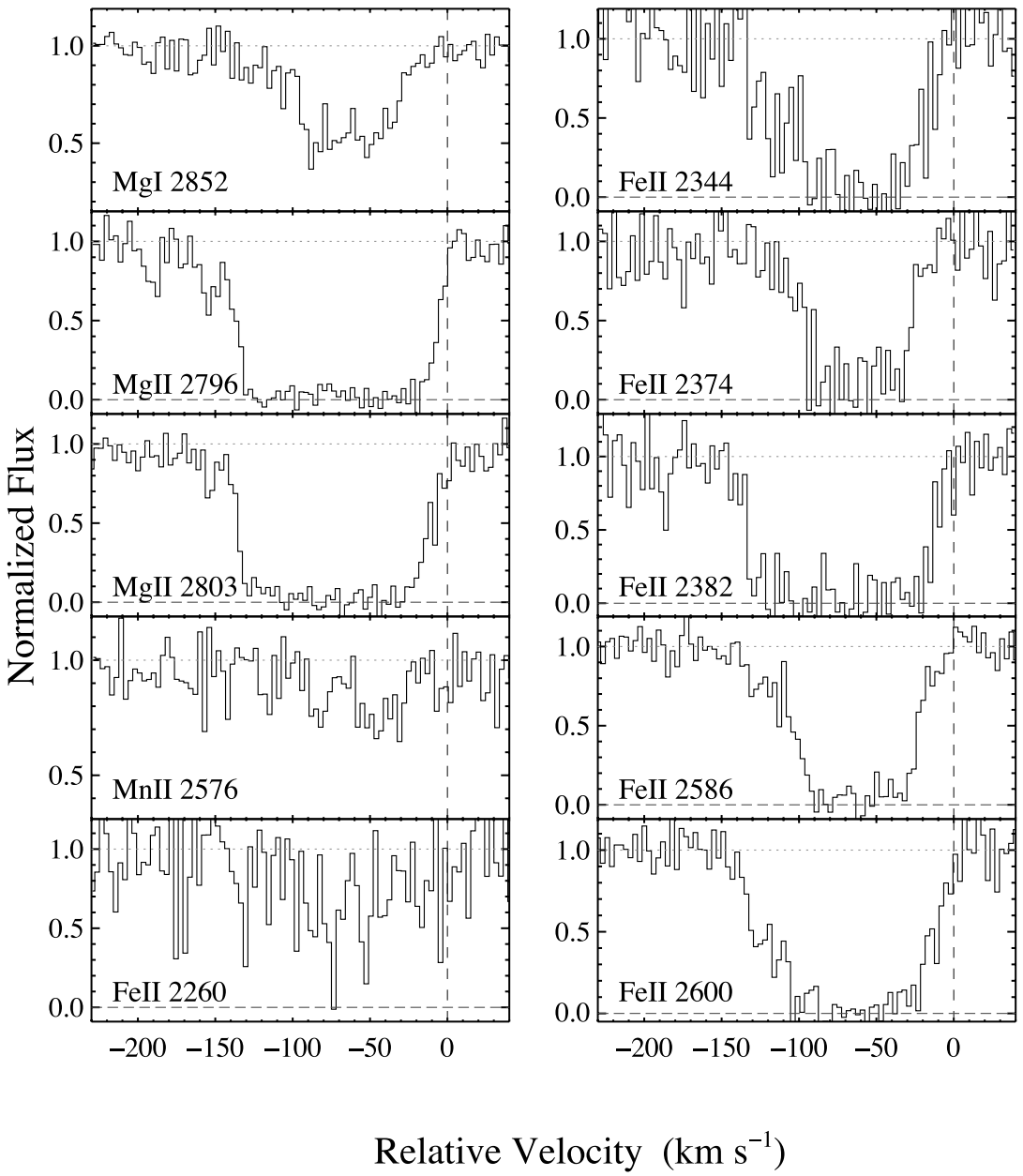

FIG. 16.—Velocity profiles of the transitions identified with the Mg II absorber at $z = 0.603$ toward GRB 060418. [*See the electronic edition of the Supplement for a color version of this figure.*]

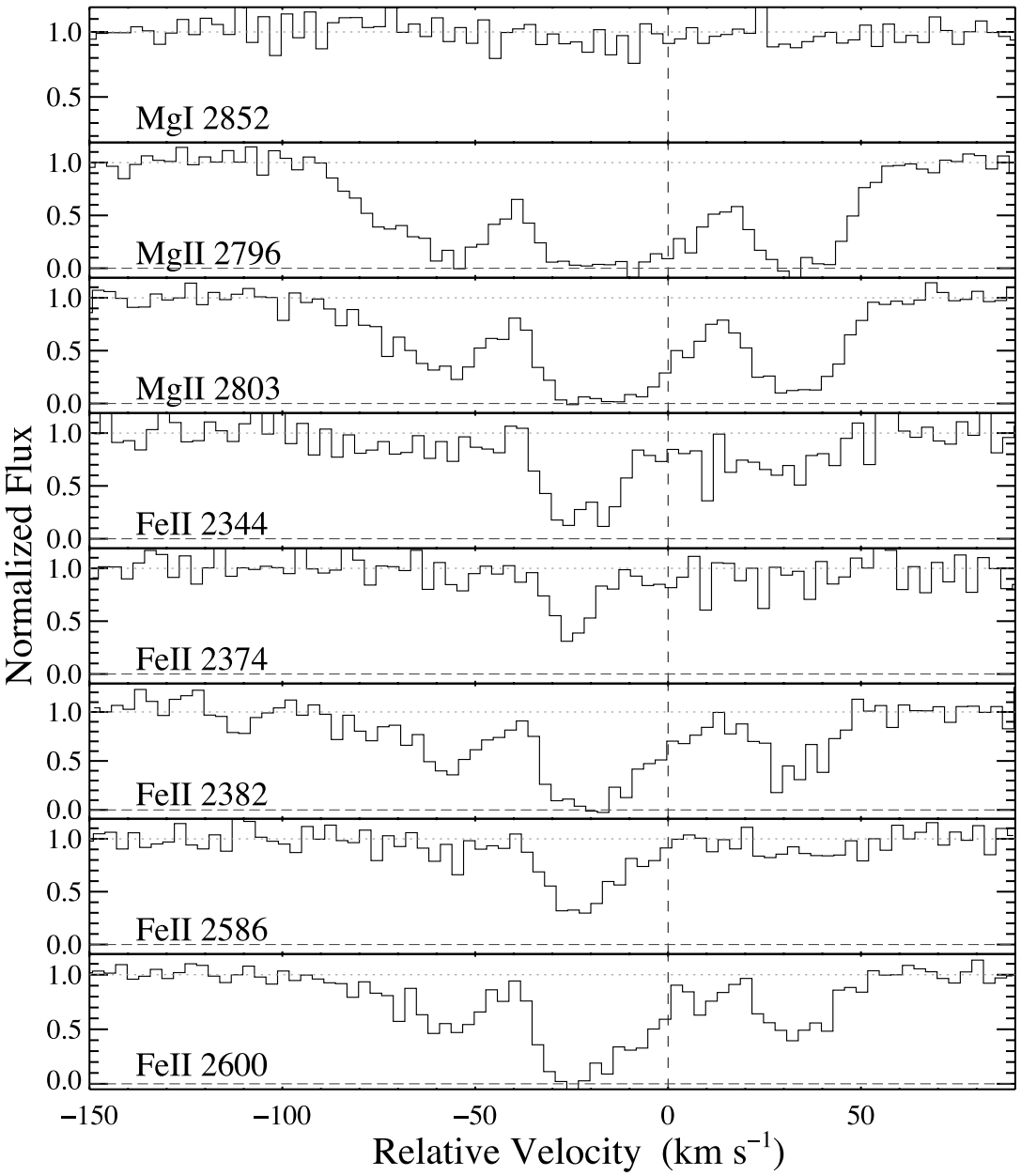

FIG. 17.—Velocity profiles of the transitions identified with the Mg II absorber at $z = 0.656$ toward GRB 060418. [*See the electronic edition of the Supplement for a color version of this figure.*]

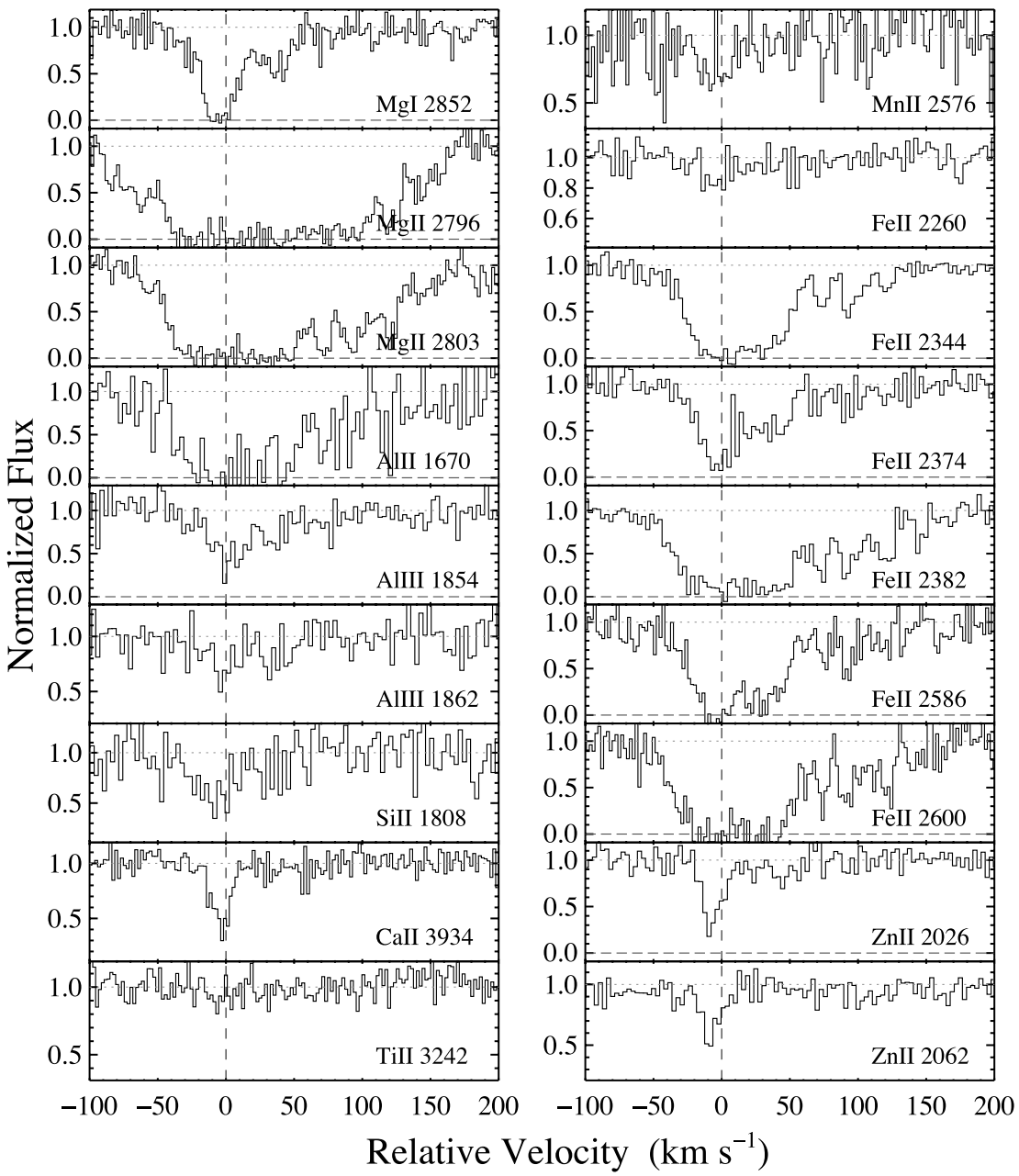

FIG. 18.—Velocity profiles of the transitions identified with the Mg II absorber at $z = 1.107$ toward GRB 060418. [*See the electronic edition of the Supplement for a color version of this figure.*]

TABLE 7

IONIC COLUMN DENSITIES FOR GRB 050730 Mg II $z = 1.773$

Ion	λ (Å)	$\log f$	$v_{\rm int}$[a] (km s^{-1})	W_λ[b] (mÅ)	$\log N$	$\log N_{\rm adopt}$
Mg I	2852.9642	0.2577	[−80, 90]	115.1 ± 34.4	12.14 ± 0.10	12.15 ± 0.10
Mg II	2796.3520	−0.2130	[−80, 90]	943.6 ± 22.7	>13.79	>14.02
	2803.5310	−0.5151	[−80, 90]	797.5 ± 21.7	>14.02	
Fe II	2260.7805	−2.6126	[−80, 90]	<53.9	<14.88	14.02 ± 0.03
	2344.2140	−0.9431	[−80, 90]	264.8 ± 22.5	13.93 ± 0.06	
	2374.4612	−1.5045	[−80, 90]	311.6 ± 20.6	<14.42	
	2382.7650	−0.4949	[−80, 90]	398.7 ± 19.1	>13.80	
	2586.6500	−1.1605	[−80, 90]	312.9 ± 19.0	14.06 ± 0.03	
	2600.1729	−0.6216	[−80, 90]	436.9 ± 23.0	>13.85	

[a] Velocity interval over which the equivalent width and column density are measured.
[b] Rest equivalent width.

TABLE 8

IONIC COLUMN DENSITIES FOR GRB 050730 Mg II $z = 2.253$

Ion	λ (Å)	$\log f$	$v_{\rm int}$[a] (km s^{-1})	W_λ[b] (mÅ)	$\log N$	$\log N_{\rm adopt}$
Mg I	2852.9642	0.2577	[−60, 120]	471.6 ± 33.0	12.71 ± 0.04	12.71 ± 0.04
Mg II	2796.3520	−0.2130	[−60, 120]	886.4 ± 31.1	>13.74	>13.97
	2803.5310	−0.5151	[−60, 130]	825.7 ± 38.4	>13.97	
Fe II	2260.7805	−2.6126	[−50, 120]	<41.8	<14.76	>14.55
	2374.4612	−1.5045	[−50, 120]	255.1 ± 27.2	>14.55	
	2382.7650	−0.4949	[−50, 120]	738.2 ± 26.5	>14.11	
	2586.6500	−1.1605	[−50, 120]	282.0 ± 25.2	>14.38	
	2600.1729	−0.6216	[−20, 120]	424.7 ± 23.7	>13.87	

[a] Velocity interval over which the equivalent width and column density are measured.
[b] Rest equivalent width.

TABLE 9

IONIC COLUMN DENSITIES FOR GRB 050820 Mg II $z = 0.692$

Ion	λ (Å)	$\log f$	$v_{\rm int}$[a] (km s^{-1})	W_λ[b] (mÅ)	$\log N$	$\log N_{\rm adopt}$
Mg II	2796.3520	−0.2130	[−480, 180]	2991.9 ± 27.5	>14.28	>14.40
	2803.5310	−0.5151	[−480, 180]	2343.0 ± 30.5	>14.40	
Ca II	3934.7770	−0.1871	[−200,0]	210.3 ± 22.1	12.49 ± 0.04	12.52 ± 0.03
	3969.5910	−0.4921	[−200,0]	140.0 ± 16.5	12.56 ± 0.05	
Fe II	2344.2140	−0.9431	[−450, 150]	1229.6 ± 52.6	>14.65	>14.65
	2382.7650	−0.4949	[−480, 180]	1722.5 ± 47.3	>14.31	

[a] Velocity interval over which the equivalent width and column density are measured.
[b] Rest equivalent width.

TABLE 10

IONIC COLUMN DENSITIES FOR GRB 050820 Mg II $z = 1.430$

Ion	λ (Å)	$\log f$	$v_{\rm int}$[a] (km s^{-1})	W_λ[b] (mÅ)	$\log N$	$\log N_{\rm adopt}$
Mg I	2852.9642	0.2577	[−200, 150]	935.1 ± 105.5	11.74 ± 0.11	11.74 ± 0.11
Mg II	2796.3520	−0.2130	[−80, 180]	1935.7 ± 134.2	>13.45	>14.20
	2803.5310	−0.5151	[−200, 180]	1084.2 ± 20.0	>14.20	
Fe II	2260.7805	−2.6126	[−200, 100]	<27.7	<14.59	14.29 ± 0.03
	2344.2140	−0.9431	[−200, 150]	365.4 ± 18.4	>14.24	
	2374.4612	−1.5045	[−200, 150]	193.0 ± 14.6	14.29 ± 0.03	
	2382.7650	−0.4949	[−200, 150]	557.4 ± 17.0	>13.95	
	2586.6500	−1.1605	[−200, 150]	391.1 ± 15.8	>14.33	
	2600.1729	−0.6216	[−200, 150]	533.4 ± 17.2	>14.03	

[a] Velocity interval over which the equivalent width and column density are measured.
[b] Rest equivalent width.

TABLE 11

IONIC COLUMN DENSITIES FOR GRB 051111 Mg II $z = 1.189$

Ion	λ (Å)	$\log f$	$v_{\rm int}$[a] (km s^{-1})	W_λ[b] (mÅ)	$\log N$	$\log N_{\rm adopt}$
Mg I.....	2852.9652	0.2577	[−130, 180]	490.7 ± 10.2	12.69 ± 0.01	12.69 ± 0.01
Mg II.....	2796.3520	−0.2130	[−130, 180]	2027.2 ± 10.0	>14.27	>14.49
	2803.5310	−0.5151	[−130, 180]	1719.2 ± 9.1	>14.49	
Ti II.....	3242.9290	−0.6345	[0, 150]	<17.4	12.13 ± 0.13	12.14 ± 0.13
Fe II	2260.7805	−2.6126	[−130, 180]	49.7 ± 12.2	<14.76	14.45 ± 0.02
	2344.2140	−0.9431	[−130, 180]	817.3 ± 10.9	>14.48	
	2374.4612	−1.5045	[−130, 180]	316.5 ± 13.4	14.45 ± 0.02	
	2382.7650	−0.4949	[−130, 180]	1184.8 ± 11.2	>14.33	
	2600.1729	−0.6216	[−130, 180]	1288.0 ± 13.7	>14.39	
Zn II.....	2026.1360	−0.3107	[0, 150]	48.7 ± 11.1	<12.56	<12.56

[a] Velocity interval over which the equivalent width and column density are measured.
[b] Rest equivalent width.

TABLE 12

IONIC COLUMN DENSITIES FOR GRB 060418 Mg II $z = 0.603$

Ion	λ (Å)	$\log f$	$v_{\rm int}$[a] (km s^{-1})	W_λ[b] (mÅ)	$\log N$	$\log N_{\rm adopt}$
Mg I.....	2852.9652	0.2577	[−180, 30]	383.3 ± 14.4	12.58 ± 0.02	12.58 ± 0.02
Mg II.....	2796.3520	−0.2130	[−180, 30]	1270.4 ± 13.4	>14.03	>14.29
	2803.5310	−0.5151	[−180, 30]	1214.7 ± 13.9	>14.29	
Mn II.....	2576.8770	−0.4549	[−100, 30]	140.2 ± 15.3	12.89 ± 0.05	12.89 ± 0.05
Fe II	2260.7805	−2.6126	[−180, 30]	311.1 ± 40.6	>15.67	>15.67
	2344.2140	−0.9431	[−180, 30]	711.9 ± 27.4	>14.53	
	2374.4612	−1.5045	[−180, 30]	579.3 ± 26.4	>14.96	
	2382.7650	−0.4949	[−180, 30]	943.3 ± 25.6	>14.23	
	2586.6499	−1.1605	[−180, 30]	737.8 ± 15.9	>14.73	
	2600.1729	−0.6216	[−180, 30]	938.6 ± 16.9	>14.31	

[a] Velocity interval over which the equivalent width and column density are measured.
[b] Rest equivalent width.

TABLE 13

IONIC COLUMN DENSITIES FOR GRB 060418 Mg II $z = 0.656$

Ion	λ (Å)	$\log f$	$v_{\rm int}$[a] (km s^{-1})	W_λ[b] (mÅ)	$\log N$	$\log N_{\rm adopt}$
Mg I.....	2852.9652	0.2577	[−100, 60]	<26.8	<11.50	<11.50
Mg II.....	2796.3520	−0.2130	[−100, 60]	972.5 ± 9.9	>13.81	>13.95
	2803.5310	−0.5151	[−100, 60]	793.9 ± 10.6	>13.95	
Fe II	2260.7805	−2.6126	[−100, 60]	<56.8	<14.92	13.86 ± 0.02
	2344.2140	−0.9431	[−100, 60]	298.7 ± 19.7	13.92 ± 0.04	
	2374.4612	−1.5045	[−100, 60]	107.9 ± 18.9	13.99 ± 0.07	
	2382.7650	−0.4949	[−100, 60]	460.0 ± 17.7	>13.76	
	2586.6499	−1.1605	[−100, 60]	196.7 ± 14.2	13.81 ± 0.03	
	2600.1729	−0.6216	[−100, 60]	491.1 ± 12.1	>13.84	

[a] Velocity interval over which the equivalent width and column density are measured.
[b] Rest equivalent width.

TABLE 14
Ionic Column Densities for GRB 060418 Mg II $z = 1.107$

Ion	J[a]	E_J (cm^{-1})	λ (Å)	log f	v_{int}[b] (km s^{-1})	W_λ[c] (mÅ)	log N	log N_{adopt}
Mg I		0.00	2852.9642	0.2577	[−80, 100]	469.5 ± 16.7	>12.90	>12.90
Mg II		0.00	2796.3520	−0.2130	[−120, 200]	1841.4 ± 22.6	>14.09	>14.32
		0.00	2803.5310	−0.5151	[−120, 200]	1536.1 ± 20.1	>14.32	
Al II		0.00	1670.7874	0.2742	[−100, 200]	738.0 ± 42.4	>13.52	>13.52
Al III		0.00	1854.7164	−0.2684	[−50, 100]	198.5 ± 14.2	13.22 ± 0.04	13.20 ± 0.03
		0.00	1862.7895	−0.5719	[−50, 100]	96.0 ± 14.4	13.16 ± 0.06	
Si II	1/2	0.00	1808.0130	−2.6603	[−70, 50]	123.8 ± 16.2	15.43 ± 0.06	15.43 ± 0.06
Ca II		0.00	3934.7770	−0.1871	[−50, 50]	144.4 ± 12.9	12.34 ± 0.03	12.34 ± 0.04
Ti II	1/2	0.00	3242.9290	−0.6345	[−50, 50]	<23.4	<12.23	<11.97
	1/2	0.00	3384.7400	−0.4461	[−50, 50]	<21.9	<11.97	
Cr II		0.00	2056.2539	−0.9788	[−50, 50]	<18.4	<12.86	<12.86
Mn II		0.00	2576.8770	−0.4549	[−50, 50]	121.1 ± 20.2	12.87 ± 0.08	12.82 ± 0.06
		0.00	2594.4990	−0.5670	[−50, 50]	76.3 ± 17.0	12.78 ± 0.09	
Fe II	9/2	0.00	2260.7805	−2.6126	[−50, 50]	45.7 ± 7.9	14.66 ± 0.07	14.66 ± 0.02
	9/2	0.00	2344.2140	−0.9431	[−80, 150]	769.3 ± 12.1	>14.56	
	9/2	0.00	2374.4612	−1.5045	[−80, 150]	433.1 ± 18.0	14.66 ± 0.03	
	9/2	0.00	2382.7650	−0.4949	[−80, 150]	1005.6 ± 15.5	>14.16	
	9/2	0.00	2600.1729	−0.6216	[−80, 150]	1104.6 ± 25.1	>14.27	
Ni II		0.00	1741.5531	−1.3696	[−50, 50]	<35.1	<13.75	<13.75
Zn II		0.00	2026.1360	−0.3107	[−50, 50]	118.6 ± 8.9	12.98 ± 0.03	12.96 ± 0.03
		0.00	2062.6640	−0.5918	[−50, 40]	70.0 ± 7.7	12.95 ± 0.05	

[a] Total angular momentum of the electron spin and orbital angular moment. The quantity E_J is the energy above the ground state.
[b] Velocity interval over which the equivalent width and column density are measured.
[c] Rest equivalent width.

Figure 7 shows the velocity profiles for the resonance lines associated with the ISM of the host galaxy. Figure 8 shows the fine-structure transitions and a resonance line for comparison. Finally, Table 4 lists the column density measurements for all of the transitions. Penprase et al. (2006) have also presented an analysis of the same HIRES data acquired for this sight line. Although our central values are generally in good agreement with their results, we report significantly smaller uncertainties, perhaps because of differences in co-adding the data.

4.4. *GRB 060418*

The *Swift* BAT instrument triggered on GRB 060418 at UT 2006 April 18 03:06:08 (Falcone et al. 2006). The satellite reported an immediate XRT position, and Falcone et al. (2006) reported a bright, optical afterglow at R.A. = $15^h45^m42.8^s$, decl. = $-03^\circ38'26.1''$. We began observations shortly after this announcement.

Figure 9 shows the velocity profiles for the resonance lines associated with the ISM of the host galaxy. Figure 10 shows the fine-structure transitions and a resonance line for comparison. Finally, Table 5 lists the column density measurements for all of the transitions.

4.5. *Summary*

Table 6 presents a summary of the gas-phase abundances observed along the four sight lines. In those cases where the $N_{H\,II}$ value was not measured (GRB 051111, GRB 060418), we have assumed a conservative upper limit of 10^{23} cm^{-2}. The relative gas-phase abundances [X/Fe] and [X/α] assume solar relative abundances (Asplund et al. 2005) and do not include ionization corrections nor differential depletion corrections.

5. STRONG, INTERVENING M II ABSORBERS

In a companion paper (Prochter et al. 2006), we have shown that there is an enhancement of strong Mg II absorbers along GRB sight lines in comparison with QSO sight lines. Here we present the full set of velocity profiles and column density measurements for the absorbers along the four GRB sight lines considered in that paper. In Figures 11–18 we present the Mg II absorption systems with $W_r > 0.5$ Å. The ionic column densities and

TABLE 15
Mg II Summary Table

GRB	z	W_λ (Å)	$N(Fe^+)$	$N(Zn^+)$	$N(Mg^0)$	$N_{H\,II}$[a]	D[b]
050730	1.773	943.6	14.02 ± 0.03		12.15 ± 0.10	18.5	7.8
050730	2.253	886.4	>14.55		12.71 ± 0.04	19.0	7.2
050820	0.692	2991.9	>14.65			19.1	7.8
050820	1.430	1935.7	14.29 ± 0.03		11.74 ± 0.11	18.8	8.1
051111	1.189	2027.2	14.45 ± 0.02	<12.56	12.69 ± 0.01	19.0	8.5
060418	0.603	1270.4	>15.67		12.58 ± 0.02	20.2	8.2
060418	0.656	972.5	13.86 ± 0.02		<11.50	18.4	7.2
060418	1.107	1841.4	14.66 ± 0.02	12.96 ± 0.03	>12.90	20.3	7.5

[a] Minimum $N_{H\,II}$ value based on the measured Fe^+ and/or Zn^+ column densities, assuming the metallicity is subsolar.
[b] D statistic (Ellison 2006), where values larger than 6.8 indicate a greater likelihood that the absorber has log $N_{H\,II} > 20.3$.

equivalent widths are reported in Tables 7–14. We have measured the D statistics (Ellison 2006) for each profile and find $D > 6.8$ in every case. This suggests that a significant fraction (>50%) of the absorbers are damped Lyα systems. In Table 15 we present a summary of these quantities. This includes the minimum $N_{\rm H\,II}$ value implied by the observed ionic column densities. In general, the values further support the conclusion that the majority of these absorbers are DLA systems.

The authors wish to recognize and acknowledge the very significant cultural role and reverence that the summit of Mauna Kea has always had within the indigenous Hawai'ian community. We are most fortunate to have the opportunity to conduct observations from this mountain. We acknowledge the efforts of S. Vogt, G. Marcy, J. Wright, and K. Hurley in obtaining the observations of GRB 050820. J. X. P. is partially supported by NASA/*Swift* grant NNG05GF55G.

REFERENCES

Asplund, M., Grevesse, N., & Sauval, A. J. 2005, in ASP Conf. Ser. 336, Cosmic Abundances as Records of Stellar Evolution and Nucleosynthesis, ed. T. G. Barnes & F. N. Bash (San Francisco: ASP), 25
Barthelmy, S. D., et al. 2005, Space Sci. Rev., 120, 143
Bergeson, S. D., & Lawler, J. E. 1993, ApJ, 414, L137
Bergeson, S. D., Mullman, K. L., & Lawler, J. E. 1994, ApJ, 435, L157
———. 1996, ApJ, 464, 1050
Bernstein, R., et al. 2003, Proc. SPIE, 4841, 1694
Chen, H.-W., et al. 2005, ApJ, 634, L25
Ellison, S. L. 2006, MNRAS, 368, 335
Falcone, A. D., et al. 2006, GCN Circ., 4966, http://gcn.gsfc.nasa.gov/gcn/gcn3/4966.gcn3
Fiore, F., et al. 2005, ApJ, 624, 853
Fox, D. B., & Cenko, S. B. 2005, GCN Circ., 3829, http://gcn.gsfc.nasa.gov/gcn/gcn3/3829.gcn3
Gehrels, N., et al. 2004, ApJ, 611, 1005
Hill, G., et al. 2005, GCN Circ., 4255, http://gcn.gsfc.nasa.gov/gcn/gcn3/4255.gcn3
Holland, S. T., et al. 2005, GCN Circ., 3704, http://gcn.gsfc.nasa.gov/gcn/gcn3/3704.gcn3
Jenkins, E. B. 1996, ApJ, 471, 292
Kulkarni, S. R., et al. 1999, Nature, 398, 389
La Parola, V., et al. 2005, GCN Circ., 4261, http://gcn.gsfc.nasa.gov/gcn/gcn3/4261.gcn3
Morton, D. C. 1991, ApJS, 77, 119
———. 2003, ApJS, 149, 205
Osborne, J. P., et al. 2005, Proc. SPIE, 5898, 352
Page, M., et al. 2005, GCN Circ., 3830, http://gcn.gsfc.nasa.gov/gcn/gcn3/3830.gcn3
Penprase, B. E., et al. 2006, ApJ, 646, 358
Prochaska, J. 2006, ApJ, 650, 272
Prochaska, J. X., Herbert-Fort, S., & Wolfe, A. M. 2005, ApJ, 635, 123
Prochaska, J. X., et al. 2001, ApJS, 137, 21
———. 2003, ApJS, 147, 227
Prochter, G. E., et al. 2006a, ApJ, 648, L93
Raassen, A. J. J., & Uylings, P. H. M. 1998, A&A, 340, 300
Rujopakarn, W., et al. 2005, GCN Circ., 4247, http://gcn.gsfc.nasa.gov/gcn/gcn3/4247.gcn3
Savage, B. D., & Sembach, K. R. 1991, ApJ, 379, 245
Tripp, T. M., Lu, L., & Savage, B. D. 1996, ApJS, 102, 239
Vogt, S. S., et al. 1994, Proc. SPIE, 2198, 362
———. 2005, ApJ, 632, 638
Yamaoka, K., et al. 2005, GCN Circ., 4299, http://gcn.gsfc.nasa.gov/gcn/gcn3/4299.gcn3